symmetry

MDPI

Article

A Multiple-Criteria Evaluation Model and Decision-Making Algorithm for 3D-Printed Continuous-Carbon-Fiber-Reinforced Composites Under Different Heat Treatment Conditions

Honghao Zhang [1], Shaolin Zhang [1], Wanying Zhu [2], Kui Wang [2], Yong Peng [2,3] and Lingyu Wang [1,*]

[1] Key Laboratory of High Efficiency and Clean Mechanical Manufacture (Ministry of Education), School of Mechanical Engineering, Shandong University, Jinan 250061, China; honghao_zhang@sdu.edu.cn (H.Z.); zsl10162022@mail.sdu.edu.cn (S.Z.)

[2] Key Laboratory of Traffic Safety on Track of Ministry of Education, School of Traffic and Transportation Engineering, Central South University, Changsha 410075, China; wanying.zhu@csu.edu.cn (W.Z.); kui.wang@csu.edu.cn (K.W.); yong_peng@csu.edu.cn (Y.P.)

[3] Joint International Research Laboratory of Key Technology for Rail Traffic Safety, Central South University, Changsha 410075, China

* Correspondence: wly202214329xzq@mail.sdu.edu.cn

Abstract

3D printing has become a revolutionary technology, and one of its major advances is the ability to continuously print objects with carbon-fiber-reinforced composites. However, to meet engineering requirements, material selection requires compromises between conflicting criteria, e.g., thermal stability, cost, and processing parameters. Resolving such conflicts inherently requires a symmetry-oriented trade-off among these competing factors. Selecting suitable composite materials for 3D printing is a complex decision-making problem. This article investigated the mechanical performance of continuous carbon fiber (CCF, as the reinforcement) polyamide composites under various heat treatment conditions. The materials were systematically evaluated by incorporating their mechanical performance, environmental, economic, and social impacts, thereby establishing a comprehensive criteria hierarchy. The mechanical responses at four heat treatment temperatures were incorporated into the decision model. An integrated multi-criteria decision method incorporating the fuzzy full consistency method (FUCOM), indifference threshold-based attribute ratio analysis (ITARA) and the fuzzy multi-attributive border approximation area comparison (MABAC) method was proposed to solve the selection problem of 3D-printed composites. The symmetry-oriented integration of subjective expert judgments and objective information allowed both information sources to jointly contribute to the determination of the composite weights. The model and method were validated using the floor of a high-speed train as a case study, and the results showed that separated-distribution CCF-reinforced composite (S-CCFRC) heat-treated at 50 °C for 4 h was the optimal solution for this engineering context. This research provides a useful tool for selecting composite materials, thereby laying the foundation for optimizing the decision-making process and further advancing research on 3D-printed composite materials.

Keywords: 3D-printed composites; mechanical properties; material selection

Academic Editor: Jie Yang

Received: 13 June 2026

Revised: 10 July 2026

Accepted: 13 July 2026

Published: 15 July 2026

1. Introduction

Manufacturing has historically served as one of the key drivers of global economic development and the advancement of urbanization in all countries. However, traditional manufacturing processes have faced a number of challenges, including high costs, long production cycles, and limited customization capabilities. To address these challenges and to drive innovation and development in manufacturing, 3D-printing technology has emerged [1]. 3D printing is a way to fabricate complex 3D physical structures through the successive layering of material based on a digital model [2]. When evaluated against the benchmark of traditional manufacturing, 3D printing is highly customizable and flexible. 3D printing allows for almost unlimited complexity and innovation. In addition, 3D printing is able to reduce material waste. With continuous technological advancements and the growing range of its applications, 3D printing has emerged as a practical tool for modern technological innovation and industry, attracting significant attention from researchers in related fields [3]. For example, the technological maturity of 3D printing is evidenced by its successful integration into diverse industrial sectors, such as the automotive, aerospace, construction, and design sectors, where it has yielded substantial economic benefits [4].

Composite materials are widely used due to their good performance, and many energy-absorbing and load-bearing structures have been gradually replaced by composites [5]. But with the development of society and the continuous improvement of requirements for products, the contradiction between the performance advantages of composites and structural efficiency is increasingly prominent. 3D printing [6] has opened up a new way for the design and manufacture of high-performance complex composite material structures. In addition, the selection of composite materials is also one of the key factors in determining the performance and quality of the product. Since these selections govern the mechanical properties and durability of a design, they are essential for meeting technical specifications and ensuring product reliability. This task is also challenging, as a wide range of material alternatives exist, each involving distinct manufacturing processes and conflicting attributes from multiple design perspectives. Furthermore, the design parameters and the various attributes exhibit complex interrelationships. Consequently, selecting the most effective alternative requires a comprehensive evaluation of a range of indices to ensure the final choice aligns with the necessities of particular use cases. Decision makers must weigh various parameters carefully to identify the most suitable candidate for a given project [7]. Existing studies on composite material selection commonly consider economic, environmental, social, and mechanical aspects as important evaluation dimensions. Additive manufacturing, when utilizing short and continuous fibers, departs from traditional processes by exerting a considerable impact on the economic and social dimensions of 3D-printed products, in addition to altering their mechanical performance. Furthermore, environmental attributes constitute a critical consideration within the prevailing framework of sustainable development [8]. Hence, choosing composites for 3D printing constitutes a complex multi-criteria decision making (MCDM) problem [9].

Among various types of 3D-printed composites, continuous-carbon-fiber-reinforced composites have attracted increasing attention due to their superior mechanical performance and potential use in load-bearing structural applications. However, their material selection remains challenging because their performance is strongly influenced by heat treatment conditions and involves multiple evaluation dimensions.

This paper investigates the mechanical properties of short carbon fiber and continuous carbon fiber (CCF) composite polyamide-based composites based on heat treatment conditions and establishes a multi-perspective index structure system for composites related to economic, environmental, social, and mechanical aspects. A comprehensive solution method containing the fuzzy full consistency method (FUCOM), indifference threshold-based attribute ratio analysis (ITARA) method and the fuzzy multi-attributive border

https://doi.org/10.3390/sym18071197

approximation area comparison (MABAC) method is proposed. To address the subjectivity of traditional weighting methods, combining subjective methods and objective methods, this paper proposes a triangular fuzzy number (TFN)–FUCOM–ITARA method for reducing the subjective influence of experts. Finally, a case study involving a high-speed train floor is conducted to validate the effectiveness and applicability of the proposed method under practical engineering conditions.

2. Literature Review

2.1. Mechanical Properties and Related Heat Treatment of 3D-Printed Composites

Owing to their outstanding mechanical properties, recyclability, and promising use in lightweight structural designs, continuous-fiber-reinforced thermoplastic polymers (CFRTPs) are emerging as viable substitutes for conventional polymeric and metallic materials [10]. The embedment of continuous fibers into 3D-printed polymers has been recognized as a very promising innovation and research hotspot for the fabrication of high-performance CFRTPs with complex geometries structures [11]. However, most 3D-printed composites still face significant challenges before they can become mainstream functional components [12]. Dickson et al. [13] examined how the incorporation of various continuous fibers influences the mechanical characteristics of 3D-printed PA composites. The findings indicated that the enhancement in tensile strength became less pronounced as fiber content continued to rise, due to insufficient interfacial adhesion between the fiber and matrix layers, coupled with the presence of increased levels of air voids with fiber content. Justo et al. [14] further confirmed that the tensile and compression properties of CFRTPs prepared by the FFF process were lower than those of the common prepregs by a vacuum bag and autoclave due to the high porosity of 3D-printed parts. Previous research [15] has identified that the key limitations that constrain the mechanical performance of 3D-printed components are their high porosity and poor interfacial adhesion, which still remain to be solved.

As an efficient post-processing technique, heat treatment has been increasingly investigated and utilized in the fabrication of conventional continuous fiber composites [16]. However, in the field of 3D-printing manufacturing, research reports have been limited to some pure polymers and short-fiber-reinforced polymers [17,18]. Basgul et al. [19] investigated how annealing influences the interfacial bonding and overall structural soundness of 3D-printed polyetheretherketone (PEEK) implants for spinal lumbar cages. Akhoundi et al. [20] explored how nozzle temperature and post-fabrication heat treatment influence the mechanical performance of high-temperature PLA manufactured through the FDM process. Furthermore, Bhandari et al. [21] aimed to enhance the interlayer tensile strength of 3D-printed composites containing SCF within PETG and PLA matrices by employing an annealing treatment. The results demonstrated that thermal post-processing influences the porosity, degree of polymer crystallization, bonding between and within layers, as well as the comprehensive mechanical performance of additively manufactured composite materials. Prior research has predominantly focused on examining how thermal post-processing affects the mechanical characteristics of 3D-printed composites. However, in practical applications, the heat treatment process itself and the social cost consumed by 3D-printing manufacturing need to be considered. Moreover, for the continuous-fiber-reinforced composites with more engineering application value, there is a certain conflict between excellent mechanical properties and high material cost. This needs to be balanced through reasonable and scientific methods.

https://doi.org/10.3390/sym18071197

2.2. Material Selection Problem

The selection of materials is a critical decision support tool in modern science and engineering. Whether in aerospace, automotive manufacturing, construction engineering, or medical devices, proper material selection directly affects the performance, quality, and sustainability of products [22]. In the past literature, many scholars and researchers have conducted extensive studies for different fields and applications and have proposed various methods and tools to assist in material selection decisions, e.g., green material assessment and environmental sustainability [23]. For example, Madhu et al. [24] proposed an analytical framework integrating multiple MCDM methods—such as FAHP, TOPSIS, VIKOR, and EDAS—to assess clean and renewable biomass feedstocks. The evaluation accounted for factors including volatile matter, fixed carbon, moisture content, and various environmental impact indicators. Tian et al. [25] constructed an MCDM method combining AHP and the gray correlation method to solve the problem of material selection based on target attributes such as indoor environmental characteristics. The effectiveness of the proposed method was confirmed through a practical case study involving the selection of environmentally sustainable interior finishing materials. In the field of 3D printing, Jha et al. [26] applied TOPSIS to biomedical 3D-printing material selection for orthopedic and prosthetic applications. Wang et al. [27] established a multi-criteria evaluation framework for 3D-printed polyamide-based composites and proposed a hybrid fuzzy DEMATEL–Entropy–TODIM–VIKOR method to solve the composite material selection problem. Xie et al. [28] integrated probabilistic interval-valued hesitant fuzzy sets, Choquet fuzzy integral, Shapley value, and TODIM–TOPSIS methods to address uncertainty and criterion interaction in 3D-printed composite material selection.

Many studies have currently considered multi-criteria systems in an integrated manner to construct complete indicator systems in many fields [29,30]. In general, economic, social and technical attributes are essential in material selection problems. In recent years, the growing emphasis on sustainable development has led to the choice of environmentally friendly materials emerging as a significant research focus within the field of materials science and selection. Therefore, in material selection, researchers are increasingly focusing on the aspects of material renewability, recyclability, energy consumption and environmental impact to promote sustainability and environmental protection [31]. Mechanical properties are fundamental characteristics of materials, and variations in composite parameters can significantly affect these properties, thereby greatly influencing the quality and performance of engineered structures.

The MCDM method is a class of methods widely used in decision analysis and problem solving [32]. It has the ability to identify the best candidate material among the many options available based on the needs of a particular application, from among the many indicators considered in different areas, e.g., sustainability and mechanical properties [33]. By using the MCDM methodology, researchers are able to quantify these criteria and make a comprehensive assessment to support comprehensive material selection decisions. The core theory and method of the MCDM method in the material selection problem can be broadly categorized into three main aspects: (1) evaluation index system construction; (2) weight assignment; and (3) decision rule and ranking method. For Part 2, weight assignment involves determining the importance weights of different evaluation criteria, and commonly used methods include AHP [34], FUCOM [35], DEMATEL [27], BWM [7] and ITARA [36]. Regarding Part 3, widely adopted decision-making methods can generally be classified into three types: (1) single evaluation methods, including TOPSIS [37], VIKOR [38], GRA [39], and MABAC [40]; (2) integrated methods combining several single evaluation methods, e.g., TOPSIS–GRA [41] and GRA–VIKOR [42], to achieve superior evaluative outcomes; (3) methods that apply semantic theory, e.g., fuzzy theory [43], uncertainty theory [44], and cloud model theory [45], aiming to mitigate the impact of uncertainty and personal bias during the evaluative phase.

2.3. Research Gap

The literature review indicates that composite materials have garnered significant research interest owing to their superior performance characteristics and broad application potential [46]. The selection of the best solution for 3D-printed composites under multiple conditions constitutes a complex MCDM problem. However, several key issues still exist in the field of 3D-printed composites, particularly in material selection. A literature search covering the past five years identified only three publications related to material selection for 3D-printed composites. These studies mainly focused on biomedical materials and polyamide or polyamide-based composite material selection, rather than continuous-carbon-fiber-reinforced composites. In most cases, the decision matrix is derived from expert evaluations rather than from direct experimental testing of material mechanical properties; current research has not fully addressed the interface interactions between different materials, in addition, the underlying mechanism through which heat treatment synergistically influences the macroscopic and microscopic structure, as well as the mechanical performance, of 3D-printed composites remains inadequately understood. Furthermore, prior investigations on thermal post-processing have primarily focused on unreinforced polymers and composites containing short fibers. There is a lack of heat treatment studies related to continuous-fiber composites, which are expected to be used as load-bearing parts in advanced engineering fields. In addition, many studies rely on a single weighting method. Subjective methods are prone to bias due to expert dependence, while objective methods may ignore practical decision preferences.

Based on the identified research gaps, the selection of continuous-carbon-fiber-reinforced polyamide composites for 3D printing constitutes a complex multi-criteria decision-making problem. This arises from the strong influence of heat treatment conditions on material properties and a systematic evaluation of materials across mechanical, environmental, economic, and social dimensions. Therefore, a comprehensive evaluation framework is required for robust decision-making.

This research established a structured, multi-level framework encompassing economic, environmental, social, and physical attributes to guide the material selection for 3D-printed CCF composites. Mechanical responses at four heat treatment temperatures (50 °C, 100 °C, 150 °C, and 200 °C) as well as two material stacking sequences were incorporated into the model. In addition, a combination of mechanical testing and an expert-constructed scoring matrix was used for material selection. This work performed sensitivity analysis, validation procedures, and an examination of practical significance. With an engineering application involving a high-speed train floor, this paper demonstrated that the approach performed well. This real-world application demonstrated that the logic behind the system was sound and produces reliable results.

3. Material and Multiple Criteria Model

Figure 1 illustrates the overall workflow of the present study. The proposed framework integrates experimental investigation with MCDM analysis, including specimen preparation, heat treatment and mechanical characterization, construction of the evaluation index system, weight determination, and material ranking procedures.

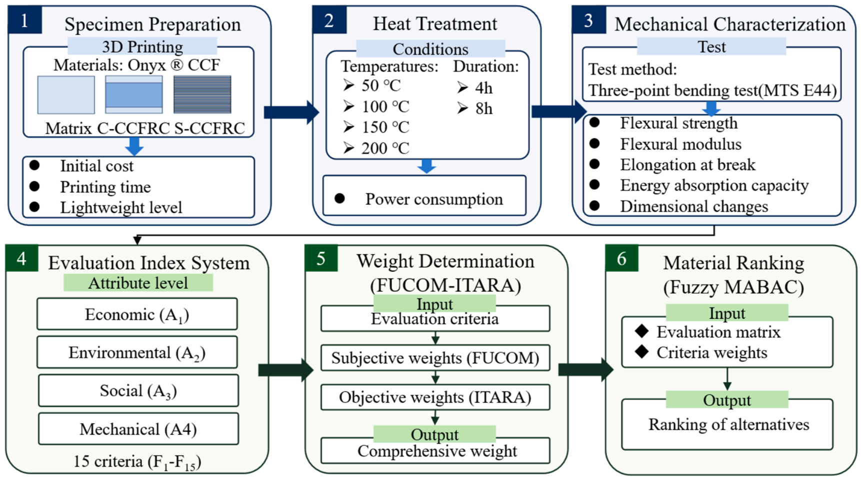

Figure 1. Overall research framework of the present study.

3.1. Material Preparation and Testing Characterization

Two filaments provided by Markforged® (Cambridge, MA, USA) were employed in this paper, one of which was Onyx® (Mark X7, Markforged, Cambridge, MA, USA). The Markforged® X7 used in this study was procured in 2018, with a build volume of 330 × 270 × 200 mm, a layer resolution of 50–250 μm, and a rated power of 150 W. The equipment market price is $69,000, and the Onyx® filament is approximately €215/800cc based on the 2018 market price from an authorized distributor. Electricity costs are calculated based on the general industrial tariff of Hunan Province (approximately 0.77 CNY/kWh for the <1 kV level, effective from September 2018). It should be noted that these economic data are primarily used for comparative evaluation among alternatives rather than for absolute cost assessment. To be more precise, each CCFRC consisted of 46 printed layers, including thirty CCF layers and sixteen functional-matrix layers, and each piece measured 90 × 6 × 6 mm. Figure 2 shows how these printed layers are stacked.

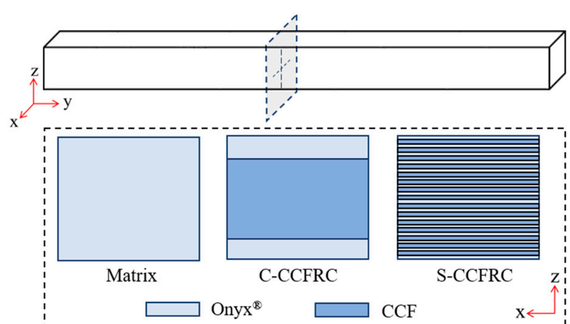

Figure 2. Schematic diagram of the stacking sequence for the three printed specimens.

It is worth noting that the slicing software Eiger® (Version 3.20.150) used with the printer was able to estimate the initial cost (material cost) and printing time of the target printed part. After printing, the specimen's weight was measured by a balance to assess the lightweight characteristic of the composite material. It can be concluded from Table 1 that compared with the matrix specimen, CCFRCs exhibited a higher initial cost, lower printing efficiency (longer printing time) and lighter weight. This stemmed from the fact that the CCF was lighter but more expensive than Onyx®, and its printing speed was slower than Onyx®. Furthermore, for CCFRCs, altering the sequence of layer deposition was found to exert minimal influence on both the initial production costs and the overall printing efficiency.

Table 1. The initial cost, lightweight level, printing time and power consumption for the printed composites under different heat treatment conditions. (50 °C–4 h denotes a heat treatment temperature of 50 °C and a heat treatment duration of 4 h, and so on.)

	Initial Cost (USD)			Printing Time (min)			Lightweight Level (g)			Power Consumption (KW/h)
	Matrix	C-CCFRC	S-CCFRC	Matrix	C-CCFRC	S-CCFRC	Matrix	C-CCFRC	S-CCFRC	
Untreated										0.00
50 °C–4 h										0.34
50 °C–8 h										0.69
100 °C–4 h	0.77	4.71	4.73	34	48	49	3.82	3.60	3.62	0.71
100 °C–8 h										1.41
150 °C–4 h										1.25
200 °C–4 h										1.98

To evaluate the effect of heat treatment duration, two representative treatment durations (4 h and 8 h) were selected for comparison. Specimens underwent heat treatment at varying temperatures (50 °C~200 °C) for durations of 4 h and 8 h, followed by natural cooling at room temperature. Due to the large dimensional deformation of specimens after 4 h heat treatment of 150 °C and 200 °C, heat treatment for 8 h was not pursued at these temperatures. Furthermore, Table 1 presents the power consumption required by heat treatment under different conditions. It was evident that an increase in the duration and temperature of heat treatment corresponded to greater power consumption.

Regarding fiber-reinforced composite materials, dimensional changes brought about by heat treatment are often limited to the direction of alignment of the fibers. In the present study, CCFs were laid to run parallel to the length of test samples (matching the Y-axis in Figure 2), which explains why dimensional shifts in the other two axes required more attention. To quantify dimensional changes, the width (aligned with the X-direction) and thickness (aligned with the Z-direction) of every specimen were recorded using electronic precision calipers, both before heat treatment and after it was completed. Then, relative changes in width and thickness were calculated, and their average values were worked out. To check how well the test samples perform mechanically, three-point bending experiments were conducted using an MTS universal mechanical testing system (model E44, made by MTS Co., MTS Systems Corporation, Eden Prairie, MN, USA); these tests were run at room temperature, with the cross-head moving at 5 mm/min. Essential mechanical parameters, including flexural strength, flexural modulus, elongation at break and energy absorption capacity, were derived from the stress–strain profiles of the additively manufactured specimens.

3.2. Property Investigation

Figure 3 illustrates the relative changes in width and thickness, as well as the flexural strength, flexural modulus, elongation at break, and energy absorption of all the printed composites. The data presented in Figure 3a,b reveal that the width and thickness of the matrix tended to decrease after heat treatment, with fluctuations restricted within a range of ±3%. The section dimensional changes of CCFRCs after 50 °C and 100 °C heat treatments were similar to those of the matrix for both 4 h and 8 h. However, unlike the matrix, the width of C-CCFRC and the thickness of S-CCFRC increased significantly after 150 °C–4 h and 200 °C–4 h heat treatment. Especially for S-CCFRC, its thickness increased by 11.81% and 16.74% after 150 °C–4 h and 200 °C–4 h heat treatment, respectively. The dimensional variations observed in CCFRCs were associated with several factors, including the ele-

https://doi.org/10.3390/sym18071197

vated porosity within CCF layers resulting from heat treatment, the specific stacking order of the CCF and matrix layers, and the interfacial adhesion between them. Furthermore, as demonstrated in Figure 3a,b, C-CCFRC exhibited superior dimensional stability under high temperatures compared to S-CCFRC, suggesting that the chosen heat treatment parameters were highly dependent on the internal architecture of the fabricated components.

As demonstrated in Figure 3c,d, appropriate thermal post-processing effectively enhanced the flexural strength and modulus of the composites; however, this enhancement did not exhibit a proportional rise with increasing treatment temperature. More specifically, the optimal mechanical performance in both the matrix and the CCFRCs was achieved following a heat treatment at 100 °C–8 h. But the improvement in flexural strength and modulus of three printed specimens was weakened after 150 °C–4 h and 200 °C–4 h heat treatment, especially in terms of the material's flexural modulus. Corresponding data for the elongation at break of the composites are presented in Figure 3e. Since the matrix with untreated, heat treated at 50 °C–4 h, 50 °C–8 h and 100 °C–4 h remained unbroken during the bending test, the elongation at break under these four conditions is not given here. In comparison to the 100 °C–4 h heat treatment, cracks appeared on the tensile side of the matrix for the 100 °C–8 h heat treatment, leading to specimen failure at a strain of 0.26. Compared with the 100 °C–4 h heat treatment, the failure strain of the matrix decreased greatly when the heating temperature increased to 150 °C and 200 °C, and the failure strain was only 0.06 under the 200 °C–4 h heat treatment. This indicated that higher heat treatment temperature or longer duration would decrease the ductility of the matrix material. For CCFRCs, the elongation at break of C-CCFRC had little change after 4 h heat treatment, but it decreased slightly after 8 h heat treatment. Similarly, the elongation at break of S-CCFRC was smaller for the 50 °C–8 h and 100 °C–8 h heat treatments than for the 50 °C–4 h and 100 °C–4 h heat treatments. The energy absorption of composites is recorded in Figure 3f. Due to its better flexural strength and modulus and the longer failure strain, the matrix exhibited the highest energy absorption for the 100 °C–8 h heat treatment. For CCFRCs, the energy absorption improved for the 150 °C and 200 °C heat treatments but decreased for the 50 °C and 100 °C heat treatments, especially when the heat treatment lasted for 8 h.

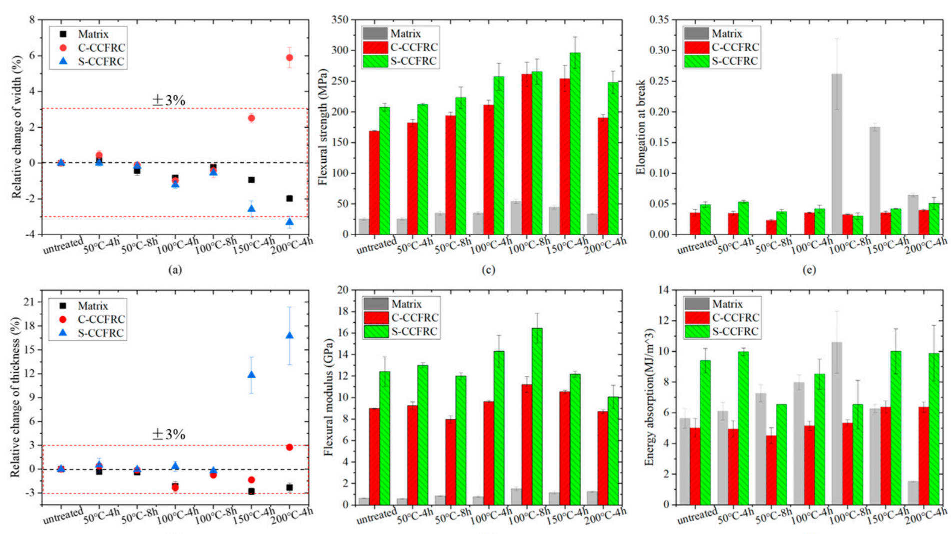

Figure 3. The dimensional changes and the flexural properties of composites under different heat treatment conditions: (**a**) relative change in width; (**b**) relative change in thickness; (**c**) flexural strength; (**d**) flexural modulus; (**e**) elongation at break; (**f**) energy absorption.

From Figure 3, it was concluded that the flexural strength and modulus, elongation at break, energy absorption and dimensional deformation of the composites could not be optimized under a single heat treatment condition. The matrix, while exhibiting low flexural strength and modulus, demonstrated good ductility, making it suitable for energy absorption during substantial deformation accumulation. Conversely, CCFRCs, despite their high flexural strength and modulus, exhibited poor ductility, rendering them suitable for rapid energy absorption under small deformation. Furthermore, S-CCFRC was superior to C-CCFRC in bending properties under almost all studied conditions, but its dimensional stability was inferior to C-CCFRC under higher heat treatment conditions.

3.3. Multiple-Criteria Model for the Selection of Composite Materials

A well-structured multi-criteria model serves as an important first step for decision-making. In this part, a decision-making framework designed for various composite materials created via additive manufacturing under different heat treatment conditions was established, as shown in Figure 4.

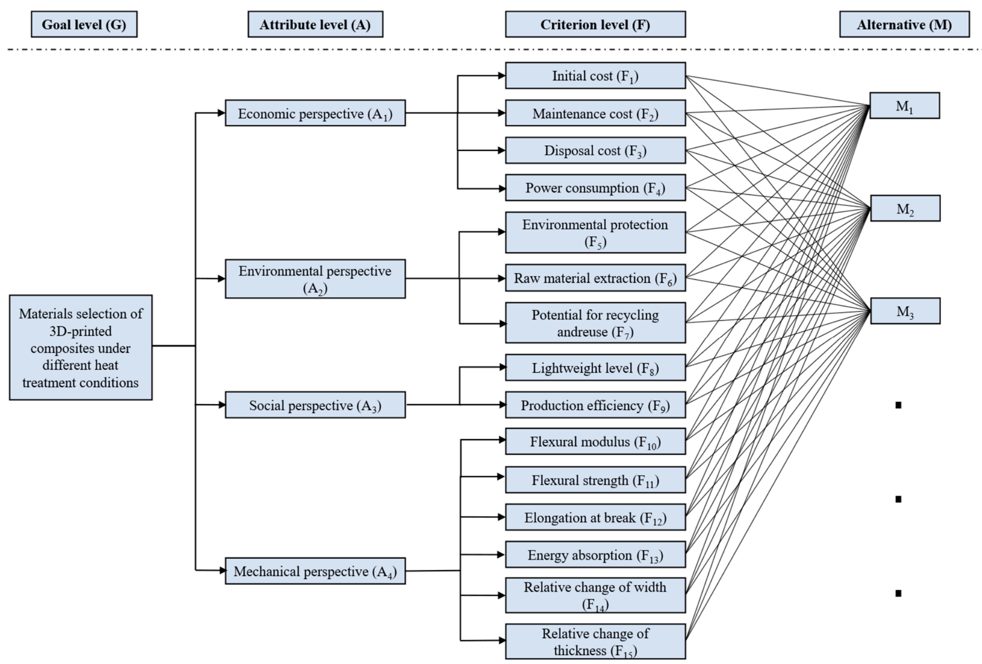

Figure 4. The multiple-criteria model.

This system was divided into four levels in a hierarchy: a goal tier, an attribute tier, a criterion tier, and an alternative tier. Appropriate heat treatment conditions for composite materials are what the goal tier (G) focuses on choosing. The attribute tier (A) includes four key areas: economic (A_1), environmental (A_2), social (A_3), and mechanical (A_4). From a symmetry-oriented perspective, these four dimensions provided a balanced and complementary representation of the economic, environmental, social, and mechanical performance of the material alternatives. The economic perspective includes initial cost (F_1), maintenance cost (F_2), disposal cost (F_3), and power consumption (F_4). The environmental perspective includes environmental protection (F_5), raw material extraction (F_6), and potential for recycling and reuse (F_7). The social perspective includes lightweight level (F_8) and production efficiency (the sum of print time and heat treatment time) (F_9). The mechanical perspective includes flexural modulus (F_{10}), flexural strength (F_{11}), elongation at break (F_{12}), energy absorption (F_{13}), relative change in width (F_{14}), and relative change in thickness (F_{15}). The alternative level considers four different heat treatment temperatures:

50 °C, 100 °C, 150 °C, and 200 °C. The system also considered the influence of the heat treatment time.

It should be emphasized that these criteria were classified into two groups: benefit-oriented and cost-oriented criteria. This classification further supported a symmetry-oriented evaluation structure. For cost-type criteria, a lower value of the criterion is better, whereas for benefit-type criteria, a higher value of the criterion is better. In the present framework, the cost-type criteria involved F_1, F_2, F_3, F_4, F_6, F_{14} and F_{15}, while the benefit type criteria involved F_5, F_7, F_8, F_9, F_{10}, F_{11}, F_{12} and F_{13}.

4. Solution Methodology

4.1. Fuzzy Set Theory

Fuzzy set theory, which was proposed by Zadeh [47], provided a new approach to address ambiguity in several disciplines such as computer science, artificial intelligence, and decision theory [48]. The triangular fuzzy number (TFN) was an extension of fuzzy theory [49]. Some definitions of the theory are given below [50,51].

Definition 1. *A fuzzy set* $\tilde{A}$ *in a universe U is an object having the form of:*

$$\tilde{A} = \left\{ \left(x, u_{\tilde{A}}(x) \right) \right\}, x \in U \tag{1}$$

where $u_{\tilde{A}}(x)$ *represents the affiliation function and U = {x} represents an aggregate of elements x. Note that a larger value of* $u_{\tilde{A}}$ *means that x belongs to the fuzzy set* $\tilde{A}$ *.*

Definition 2. *Let* $\tilde{a} = \left(a^l, a^m, a^u \right)$ *represent a TFN. The affiliation function of* $u_{\tilde{a}}(x)$ *satisfies Equation (2).*

$$u_{\tilde{a}}(x) = \begin{cases} 0, x \le a^l \\ \dfrac{x - a^l}{a^m - a^l}, a^l < x \le a^m \\ \dfrac{a^u - x}{a^u - a^m}, a^m \le x < a^u \\ 0, x \ge a^u \end{cases} \tag{2}$$

where $x \in R$, a^l *represents the lower limit of* $\tilde{a}$, a^m *represents the most likely value of* $\tilde{a}$, *and* a^u *represents the upper limit of* $\tilde{a}$. *Note that R is a real number and* $a^l \le a^m \le a^u$.

Definition 3. *Suppose that* $\tilde{a}$ = (a^l, a^m, a^u) *and* $\tilde{b}$ = (b^l, b^m, b^u) *are two TFNs, and* $\mu > 0$. *Then the operation rules can be defined as follows.*

$$\tilde{a} + \tilde{b} = \left(a^l + b^l, a^m + b^m, a^u + b^u \right) \tag{3}$$

$$\tilde{a} - \tilde{b} = \left(a^l + b^u, a^m - b^m, a^u - b^l \right) \tag{4}$$

$$\tilde{a} \times \tilde{b} = \left(a^l b^l, a^m b^m, a^u b^u \right) \tag{5}$$

$$\tilde{a} / \tilde{b} = \left(a^l / b^u, a^m / b^m, a^u / b^l \right) \tag{6}$$

$$\mu \tilde{a} = \left(\mu a^l, \mu a^m, \mu a^u \right) \tag{7}$$

Definition 4. *Let* $\tilde{a}$ *= (a^l, a^m, a^u) be a TFN. The score function* $S(\tilde{a})$ *is defined as the following:*

$$S(\tilde{a}) = \frac{a^l + 4 \times a^m + a^u}{6} \tag{8}$$

where the larger the value of $S(\tilde{a})$*, the larger the triangular fuzzy value of* $\tilde{a}$*. Note that the defuzzification results can be expressed by* $S(\tilde{a})$*.*

Definition 5. *Let* $\tilde{a}$ *= (a^l, a^m, a^u) and* $\tilde{b}$ *= (b^l, b^m, b^u) be two TFNs. The distance between them is defined as:*

$$d\left(\tilde{a},\tilde{b}\right) = \left[\frac{\left(a^l - b^l\right)^2 + \left(a^m - b^m\right)^2 + \left(a^u - b^u\right)^2}{3}\right]^{\frac{1}{2}} \tag{9}$$

Definition 6. *Let* $\tilde{x}_{1j}\left(j = 1,2,\ldots,n\right)$ *be a series of TFNs. The aggregation operator of triangular fuzzy numbers is as follows:*

$$\tilde{z}_{ij} = \left(z_{ij}^{(l)}, z_{ij}^{(m)}, z_{ij}^{(u)}\right) = \left\{\begin{array}{l} z_{ij}^{(l)} = \min\left(\tilde{x}_{ij}^{e}\right) \\ z_{ij}^{(m)} = \sqrt[k]{\Pi_{e=1}^{k}\tilde{x}_{ij}^{e}} \\ z_{ij}^{(u)} = \max\left(\tilde{x}_{ij}^{e}\right) \end{array}\right\} \tag{10}$$

where $\tilde{x}_{ij}^{e}$ *is the preference of the e-th expert and k is the total number of experts.*

4.2. Fuzzy FUCOM–ITARA Method

The FUCOM method was first introduced by Pamučar et al. [52]. FUCOM uses a simple algorithm to determine the weights of criteria and requires only a smaller number of pairwise comparisons for determining criteria weights. ITARA for the weight assignment of attributes was proposed by Hatefi [53] in multi-attribute decision problems. The ITARA method does not require information from the decision makers but obtains the weights directly from the decision matrix data. In this paper, the fuzzy FUCOM–ITARA method was proposed to obtain the correlation and importance weights of each criterion. In contrast to weighting methods that use subjective information to assign attributes, objective techniques determine weights based on objective information (e.g., a decision matrix). However, various subjective techniques may be influenced in several ways, and there is no agreement on which method yields more accurate weights. Combining subjective methods and objective methods allows the problem to be examined from multiple perspectives. The combined use of subjective and objective weighting methods supports a symmetry-oriented framework, allowing the problem to be examined from multiple perspectives by incorporating both expert judgments and data-driven information into the determination of criterion weights. The subjective technique approach allows the weights to be adjusted to specific needs and contexts, making decisions more actionable and adaptable, while the objective technique approach is based on data, reducing the influence of personal bias and improving the comprehensiveness of decisions. The method used TFNs to reduce the problem of subjectivity and uncertainty in the decision-making process [54]. The specific steps of the fuzzy FUCOM–ITARA method proposed in this paper are summarized as follows:

Step 1: Determine the priority order of criteria. The indicators are ranked from most important to least important as shown in Equation (11).

$$C_{j(1)} > C_{j(2)} > \cdots C_{j(n)} \tag{11}$$

where C_j denotes a criterion (or attribute) in a predefined set containing n indicators.

Step 2: Evaluate the relative importance between adjacent criteria. Based on the fuzzy linguistic ratings provided in Table 2, the relative importance between two neighboring indicators is determined, and the relative importance vector is formed.

$$\left[\tilde{\varphi}_{1/2}, \tilde{\varphi}_{2/3}, \cdots \tilde{\varphi}_{(n-1)/n}\right] \tag{12}$$

where $\tilde{\varphi}_{(n-1)/n}$ denotes the relative importance of $C_{j(n-1)}$ over $C_{j(n)}$. $\tilde{\varphi}_{(n-1)/n}$ is expressed in terms of fuzzy linguistic ratings.

Table 2. Fuzzy linguistic scale for the comparison.

Linguistic Variables	Equal Importance (E)	Less Important (L)	Fairly Important (F)	Very Important (V)	Absolutely Important (A)
TFN	(1, 1, 1)	(2/3, 1, 3/2)	(3/2, 2, 5/2)	(5/2, 3, 7/2)	(7/2, 4, 9/2)

Step 3: Establish constraints for subjective weights. Calculate the fuzzy weights $\tilde{w}_j = \left(w_j^l, w_j^m, w_j^u\right)$ for each indicator. The fuzzy weights should fulfill the following two conditions:

$$\frac{\tilde{w}_j}{\tilde{w}_{j+1}} = \left(\frac{w_j^l}{w_{j+1}^u}, \frac{w_j^m}{w_{j+1}^m}, \frac{w_j^u}{w_{j+1}^l}\right) = \tilde{\varphi}_{j/(j+1)} \tag{13}$$

$$\frac{\tilde{w}_j}{\tilde{w}_{j+2}} = \left(\frac{w_j^l}{w_{j+2}^u}, \frac{w_j^m}{w_{j+2}^m}, \frac{w_j^u}{w_{j+2}^l}\right) = \tilde{\varphi}_{j/(j+2)} = \tilde{\varphi}_{j/(j+1)} \otimes \tilde{\varphi}_{(j+1)/(j+2)} = \frac{\tilde{w}_j}{\tilde{w}_{j+1}} \otimes \frac{\tilde{w}_{j+1}}{\tilde{w}_{j+2}} \tag{14}$$

Step 4: Calculate subjective weights of criteria. The TFN-based fuzzy weights of each criterion and attribute are obtained by Equation (15). Then the results are defuzzified using Equation (16). Finally, the final weight of each criterion $\omega_{1j} = [\omega_{s1}, \omega_{s2}, \ldots, \omega_{sn}]$ can be obtained by multiplying the weight of the criterion by the weight of the corresponding attribute.

$$\begin{aligned}
&\min \xi \\
&s.t. \\
&\begin{cases}
\left|\dfrac{\tilde{w}_k}{\tilde{w}_{k+1}} - \tilde{\varphi}_{k/(k+1)}\right| \le \xi, \forall j \\
\left|\tilde{w}_k - \tilde{\varphi}_{k/(k+1)} \otimes \tilde{\varphi}_{(k+1)/(k+2)}\right| \le \xi, \forall j \\
\sum_{j=1}^{n} \tilde{w}_j = 1, \forall j \\
w_j^l \le w_j^m \le w_j^u \\
w_j^l \ge 0, \forall j \\
j = 1, 2, \ldots, n
\end{cases}
\end{aligned} \tag{15}$$

where ζ is the objective function under nonlinear programming.

$$S\left(\tilde{w}_j\right) = \frac{w^l + 4 \times w^m + w^u}{6} \tag{16}$$

Step 5: Construct a triangular fuzzy number decision matrix $\tilde{P} = \left[\tilde{p}_{ij}\right]_{m \times n}$.

$$\tilde{P} = \begin{array}{c} \\ A_1 \\ \vdots \\ A_m \end{array} \begin{array}{c} \begin{array}{ccc} C_1 & \cdots & C_n \end{array} \\ \begin{bmatrix} \left(a_{\tilde{P}_{11}}^l, a_{\tilde{P}_{11}}^m, a_{\tilde{P}_{11}}^u\right) & \cdots & \left(a_{\tilde{P}_{1n}}^l, a_{\tilde{P}_{1n}}^m, a_{\tilde{P}_{1n}}^u\right) \\ \vdots & \ddots & \vdots \\ \left(a_{\tilde{P}_{m1}}^l, a_{\tilde{P}_{m1}}^m, a_{\tilde{P}_{m1}}^u\right) & \cdots & \left(a_{\tilde{P}_{mn}}^l, a_{\tilde{P}_{mn}}^m, a_{\tilde{P}_{mn}}^u\right) \end{bmatrix} \end{array} \tag{17}$$

where $\tilde{P}_{ij} = \left(a^{l}_{\tilde{P}_{ij}}, a^{m}_{\tilde{P}_{ij}}, a^{u}_{\tilde{P}_{ij}}\right), (i = 1, \ldots, m; j = 1, \ldots, n)$ is a TFN that represents the aggregated assessment of the alternative A_i under the core criterion C_j.

Step 6: Construct the real decision matrix $\tilde{R} = \left[\tilde{r}_{ij}\right]_{m\times n}$.

$$r_{ij} = \frac{\dfrac{a^{l}_{\tilde{P}_{ij}} + 4\times a^{m}_{\tilde{P}_{ij}} + a^{u}_{\tilde{P}_{ij}}}{6}}{\sum_{i=1}^{m} \dfrac{a^{l}_{\tilde{P}_{ij}} + 4\times a^{m}_{\tilde{P}_{ij}} + a^{u}_{\tilde{P}_{ij}}}{6}}, i = 1, 2, \ldots, m; j = 1, 2, \ldots, n \tag{18}$$

where r_{ij} denotes the defuzzification scores of the alternative A_i under the criterion C_j.

Step 7: Normalize and rank decision values. Rank normalized performance scores R_{ij} in ascending order:

$$\rho_{(1)j} = \min_{1\le i\le m} R_{ij} < \cdots < \rho_{(m)j} = \max_{1\le i\le m} R_{ij}, j = 1, \ldots, n \tag{19}$$

where $\rho_{(1)j}$ denotes the lowest normalized performance score and $\rho_{(m)j}$ denotes the highest normalized performance score.

Step 8: Compute the ordered distances.

$$\gamma_{ij} = \rho_{i+1,j} - \rho_{ij}, \left(i = 1, \ldots, m-1; j = 1, \ldots, n\right) \tag{20}$$

where γ_{ij} represents the calculated distance between consecutive normalized aggregated performance scores $\rho_{i+1,j}$ and ρ_{ij}.

Step 9: Identify significant differences among criterion values. Define the considerable difference between γ_{ij} and τ.

$$\xi_{ij} = \begin{cases} \gamma_{ij} - \tau, \gamma_{ij} > \tau \\ 0, \quad \gamma_{ij} < \tau \end{cases} \tag{21}$$

where τ stands for normalized indifference threshold. If $\gamma_{ij} - \tau > 0$, it is essential to assign greater weight to criteria that correspond to larger sequential distances in the ranking. This means that the more dispersed the data, the greater the weight of the relevant indicator. Also, wider normalized indifference threshold should assign smaller weights to the indicator.

Step 10: Determine objective weights of criteria.

$$\omega_j = \frac{q_j}{\sum_{j=1}^{n} q_j} \tag{22}$$

where $q_j = \left(\sum_{i=1}^{m-1} \xi_{ij}^{p}\right)^{1/p}, \forall j \in N$. p, with a range between 1 and ∞, is the preferred metric. Most common and important are $p = 1$, $p = 2$, and $p = \infty$, which indicate that the requested weights are based on the Manhattan, the Euclidian, and the Tchebycheff distances, respectively. In this paper, $p = 2$.

Step 11: Obtain the comprehensive weight. The correlation and importance of each criteria are combined, and then the comprehensive weight is obtained. In this paper, a game-theoretic approach is used, it aims to reach the Nash equilibrium and effectively combines the subjective weights and objective weights to obtain the relatively scientific combination weights. The combined weight ω^* is calculated by Equation (23).

$$\omega^* = \lambda_1^*\left(\omega_{sj}\right)^T + \lambda_2^*\left(\omega_{oj}\right)^T \tag{23}$$

The optimization objective model is developed as follows:

$$\min\left\|\lambda_1 w^1 + \lambda_2 w^2 - w^k\right\|_2; \left(k = 1.2\right) \tag{24}$$

where w^1 and w^2 represent the obtained subjective and objective weights, respectively. The optimal solution of the model derived from Equation (25) needs to satisfy the following linear equation:

$$\begin{bmatrix} w^1\left(w^1\right)^T & w^1\left(w^2\right)^T \\ w^2\left(w^1\right)^T & w^2\left(w^2\right)^T \end{bmatrix}\begin{pmatrix} \lambda_1 \\ \lambda_2 \end{pmatrix}=\begin{bmatrix} w^1\left(w^1\right)^T \\ w^2\left(w^2\right)^T \end{bmatrix} \tag{25}$$

The optimal weighting factor can be obtained from the following equation:

$$\lambda_l^* = \frac{\left|\lambda_l\right|}{\sum_{p=1}^{2}\left|\lambda_p\right|};\left(l=1,2\right) \tag{26}$$

4.3. Fuzzy MABAC Method

The fundamental logic of the MABAC method involves measuring how far each alternative is from the boundary approximation area (BAA) across all evaluated criteria. Within TFN theory, this approach was applied to the composite material selection process for ranking and identifying the optimal material. This methodology allows for a precise comparison of options even when faced with the inherent vagueness of experimental data. The comprehensive procedures for the fuzzy MABAC method are outlined as follows:

Assume alternatives $S_i = \{S_1, S_2, \ldots, S_m\}$, the evaluation index system $A_j = \{A_1, A_2, \ldots, A_n\}$, and the decision makers $DM_k = \{DM_1, DM_2, \cdots, DM_l\}$. Let $\lambda = \{\lambda_1, \lambda, \ldots, \lambda_l\}$ be the weights of decision makers, meeting the requirement that $0 \le \lambda_k \le 1$ ($k = 1, 2, \cdots, l$) and $\sum_{k=1}^{l}\lambda_k = 1$. Each decision maker evaluated each criterion. After that, the evaluations were transformed into the corresponding TFNs based on linguistic variables, and the evaluation matrices $\tilde{E}_k = \left(\tilde{S}_{ij}^{(k)}\right)_{m*n} = \left(a_{ij}^{l(k)}, a_{ij}^{m(k)}, a_{ij}^{u(k)}\right)_{m*n}, k=1,2,\ldots,l$ were obtained. The linguistic terms used to evaluate the alternative solutions in this work are presented in Table 3.

Table 3. Linguistic variables for rating solutions.

Linguistic Variables	Very Low (VL)	Low (L)	Slightly Low (SL)	Medium (M)	Slightly High (SH)	High (H)	Very High (VH)
Corresponding TFN	(0, 0, 1)	(0, 1, 3)	(1, 3, 5)	(3, 5, 7)	(5, 7, 9)	(7, 9, 10)	(9, 10, 10)

Step 1: Aggregate expert evaluations and construct the fuzzy decision matrix. Utilize the $\tilde{E}_k$ forming the initial decision matrix $\left(\tilde{P}\right)$. Aggregate decision matrices by using Equation (11) to obtain $\tilde{P} = \left[\tilde{p}_{ij}\right]_{m\times n}$, where $\tilde{p}_{ij}$ is the value of the *i*-th alternative according to the *j*-th criterion ($i = 1, 2, \ldots, m$; $j = 1, 2, \ldots, n$).

Step 2: Normalize the decision matrix. Normalize the elements from the real decision matrix $R = \left[r_{ij}\right]_{m\times n}$ to obtain $V = \left[v_{ij}\right]_{m\times n}$.

$$v_{ij} = \begin{cases} \dfrac{r_{\max j} - r_{ij}}{r_{\max j} - r_{\min j}} \\ \dfrac{r_{ij} - r_{\min j}}{r_{\max j} - r_{\min j}} \end{cases} \tag{27}$$

For the cost-type criteria, $v_{ij} = \left(r_{\max j} - r_{ij}\right)/\left(r_{\max j} - r_{\min j}\right)$, and for the benefit-type criteria, $v_{ij} = \left(r_{ij} - r_{\min j}\right)/\left(r_{\max j} - r_{\min j}\right)$, where $r_{\max j}$ represents the maximum value of the *j*-th column and $r_{\min j}$ represents the minimum value of the *j*-th column.

Step 3: Construct the weighted decision matrix. Compute the weighted matrix $Z = \left(z_{ij}\right)_{m\times n}$ on the basis of Equation (28).

$$z_{ij} = \omega_j \cdot \left(v_{ij} + 1\right) \tag{28}$$

https://doi.org/10.3390/sym18071197

Step 4: Compute the BAA matrix $G = \left(g_j\right)_{1\times n}$. The BAA for each attribute is obtained by Equation (29).

$$g_j = \prod_{i=1}^{m}\left(z_{ij}\right)^{1/m} \tag{29}$$

Following the computation of the g_j value for every criterion, a border approximation area matrix (G) is constructed, which has the dimensions of 1×n.

Step 5: Calculate distances from the BAA. Compute the distance (D) of each alternative from the border approximation area for all elements in the matrix.

$$D = \begin{bmatrix} d_{11} & d_{12} & \cdots & d_{1n} \\ d_{21} & d_{22} & \cdots & d_{2n} \\ \cdots & \cdots & \cdots & \cdots \\ d_{m1} & d_{m2} & \cdots & d_{mn} \end{bmatrix} \tag{30}$$

Calculate the distance matrix $D = \left(d_{ij}\right)_{m\times n}$ using Equation (31).

$$D = Z - G = \begin{bmatrix} z_{11} & z_{12} & \cdots & z_{1n} \\ z_{21} & z_{22} & \cdots & z_{2n} \\ \cdots & \cdots & \cdots & \cdots \\ z_{m1} & z_{m2} & \cdots & z_{mn} \end{bmatrix} - \begin{bmatrix} g_1 & g_2 & \cdots & g_n \\ g_1 & g_2 & \cdots & g_n \\ \cdots & \cdots & \cdots & \cdots \\ g_1 & g_2 & \cdots & g_n \end{bmatrix} \tag{31}$$

Step 6: Compute comprehensive scores and rank alternatives. The comprehensive evaluation value Q_i for each alternative is calculated using Equation (32), defined as the summation of the distances d_i of the alternative from the border approximation area across all criteria.

$$Q_i = \sum_{j=1}^{n} d_{ij}, i = 1,2,\cdots,m; j = 1,2,\cdots,n \tag{32}$$

Rank the alternatives in descending order based on their calculated Q_i values. The alternative achieving the highest Q_i score is identified as the optimal solution.

4.4. Structural Components of the Proposed Method

A hybrid decision-making method was proposed to guide the selection of CFRCs for 3D-printing applications based on the heat treatment case. The overall procedure can be summarized in two parts, illustrated in Figure 5, while its main stages and procedures are summarized in Table 4.

Stage 1: Establish a standard criteria system and the linguistic variables assessment matrix.

To ensure that the assessment remained comprehensive, a diverse group of specialists, including academic instructors and technical professionals, contributed their insights to the decision matrix. Their feedback focused on the specific influence each index exerted on the overall system. Furthermore, the mechanical indicators were obtained from the mechanical investigation in Section 3. This integration of subjective expert opinion and objective laboratory results provided a balanced foundation for the subsequent analysis.

Stage 2: The weight vector for every evaluation criterion was calculated through the fuzzy FUCOM–ITARA approach, ensuring that each criterion was properly balanced, and the optimal solution was obtained using the fuzzy MABAC method.

For the decision matrix, the values of initial cost (F_1), power consumption (F_4), lightweight level (F_8), production efficiency (F_9), flexural modulus (F_{10}), flexural strength (F_{11}), elongation at break (F_{12}), energy absorption (F_{13}), relative change in width (F_{14}) and relative change in thickness (F_{15}) are obtained from the material tests of Sections 3.1 and 3.2. The values of other criteria are obtained by experts based on linguistic scale scores. In this study, the fuzzy decision matrix contained n evaluation criteria and m alternatives. In order to minimize the subjectivity of decision making and experimental errors, fuzzy set theory was used to represent the values of the criteria. A combination of TFN and FUCOM–ITARA was used to obtain the weight vector of each index. The fuzzy MABAC is used to calculate the Q_i values of each alternative. A higher Q_i value indicates superior overall performance. Consequently, the final ranking and the optimal selection among the 3D-printed composites were determined by comparing their respective Q_i values.

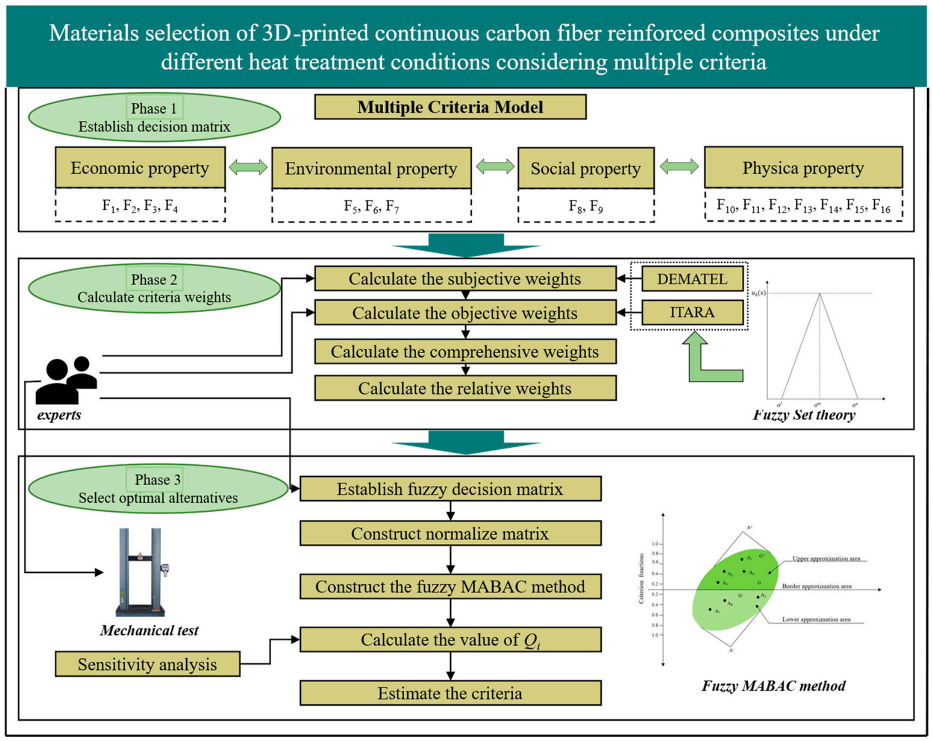

Figure 5. Comprehensive procedural map for the proposed solution method.

Table 4. Procedure of the proposed method framework.

Input	Alternative Material Information
Step 1:	Construct the hierarchical evaluation criteria system.
Step 2:	Collect quantitative data and expert evaluations.
Step 3:	Determine subjective criterion weights using the fuzzy FUCOM method.
Step 4:	Determine objective criterion weights using the fuzzy ITARA method.
Step 5:	Obtain the comprehensive weights.
Step 6:	Evaluate the alternatives using the fuzzy MABAC method.
Step 7:	Rank the alternatives and identify the optimal material.
Output	The best alternative.

5. Results and Discussion

5.1. Engineering Background

Rail transit systems offer obvious advantages in providing an efficient, reliable, environmentally friendly and comfortable way to travel around the city, and they play an important role in relieving traffic pressure and improving the urban environment. As the field of composite technology continues to evolve, polymer-based composite materials have been employed on an increasingly large scale in railroad vehicles, and the materials and manufacturing processes for trains have significantly improved, e.g., SKF of Sweden uses 25% glass-fiber-reinforced PA66 composite material to make bearing cages on locomotive traction motor bearings; the first commercial air rail train developed by CRRC

Qingdao Sifang Co., Ltd., adopted lightweight aluminum alloy material with high pressure performance. This section uses a rapid-transit railcar floor as the technical case study. The specific layout and design of this structural component are depicted in Figure 6. Composite materials can effectively reduce the body weight, and the flexibility of fiber composites can reduce production costs while also meeting aerodynamic requirements. In addition, these materials can effectively absorb impact energy and provide thermal insulation under fire and other extreme conditions, thereby ensuring passenger safety.

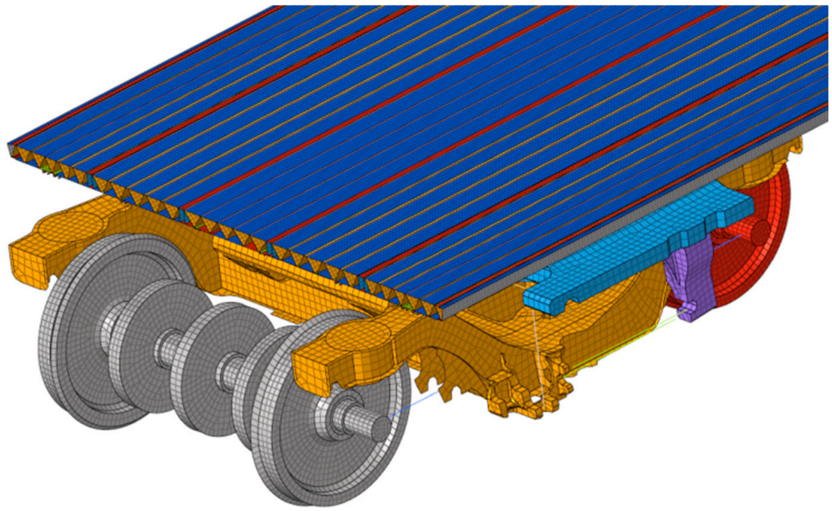

Figure 6. The floor of high-speed train.

5.2. Weight Vector of Each Criterion

A multi-criteria model was employed in this subsection, as shown in Figure 3. The prepared 3D-printed samples were studied under different heat treatment conditions. For convenience, all alternatives in the decision matrix were designated as shown in Table 5.

Table 5. The name of 3D printed composites with different heat treatment conditions and different stacking sequences.

	Matrix	C-CCFRC	S-CCFRC
Untreated	S_1	S_8	S_{15}
50 °C–4 h	S_2	S_9	S_{16}
100 °C–4 h	S_3	S_{10}	S_{17}
150 °C–4 h	S_4	S_{11}	S_{18}
200 °C–4 h	S_5	S_{12}	S_{19}
50 °C–8 h	S_6	S_{13}	S_{20}
100 °C–8 h	S_7	S_{14}	S_{21}

Three cross-disciplinary experts, E_1, E_2, and E_3, with backgrounds ranging from senior engineering practitioners to university academic researchers, were invited to participate in the evaluation process. They used fuzzy linguistic assessment levels (details in Table 3) as a basis to generate evaluation scores for decision-making. Since there are no multiple optional selections in the attribute dimension, a decision matrix was constructed by aggregating together the scores the three experts gave for different attributes; this matrix is then used to calculate the attribute weight vector through the FUCOM–ITARA method. In the decision matrix for material option screening, indicator values linked to F_1, F_4, F_8, F_9, F_{10}, F_{11}, F_{12} and F_{13} were obtained from material mechanical performance tests, while data for all other criteria were obtained from expert evaluations, with specific details shown in Table A1. Because subjective judgment in decision-making and experimental test deviations may introduce uncertainty and affect the results, this study employed TFN to construct the above-mentioned decision matrix. After aggregating the assessments from the three experts, the finalized decision matrix was obtained, as shown in Table A2. Using the analytical framework set up in Section 4.2, the weight for each attribute was determined, and the numerical values are detailed for review in Table 6.

Table 6. The fuzzy decision matrix of attributes.

Fuzzy Rating Attribute	Economic Property (A_1)	Environmental Property (A_2)	Social Property (A_3)	Mechanical Property (A_4)
E_1	M	M	SH	SH
E_2	SH	SH	M	VH
E_3	H	SH	M	M
τ	0.01	0.02	0.01	0.01
ω_j	0.2542	0.1918	0.2367	0.3173

Next, the weight vector for each criterion in the constructed model was obtained with the fuzzy FUCOM–ITARA approach. Based on the methodology proposed in Section 4.2, the importance among the indicators was shown in Table 7, and the subjective weights of the indicators were determined. Additionally, the objective weights of the indicators were solved by the expert decision matrix. Finally, a composite weight was obtained by integrating subjective and objective weights using game theory. The final weight vector was obtained by multiplying attribute weights with their corresponding criterion weights, and this vector is then used to rank each attribute and criterion by how important they are. Table 8 shows both the final weights and ranking positions of each criterion in the index system.

Table 7. The subjective judgments for determining the weights.

Item	Ranking	TFN
Four attributes	$A_4 > A_3 = A_1 > A_2$	[L, E, F]
Four economic criteria	$F_1 > F_2 > F_3 = F_4$	[F, L, E]
Three environmental criteria	$F_5 > F_7 > F_6$	[V, F]
Two social criteria	$F_8 > F_9$	[F]
Six mechanical criteria	$F_{13} > F_{11} > F_{10} > F_{14} = F_{15} > F_{12}$	[L, L, F, E, L]

Table 8. Weight and rank of each index on model.

Attribute	Weight	Criteria	Weight	Final Weight	Rank
A_1	0.2542	F_1	0.0879	0.0223	15
		F_2	0.1985	0.0505	11
		F_3	0.2108	0.0536	7
		F_4	0.5028	0.1278	2
A_2	0.1918	F_5	0.2778	0.0533	8
		F_6	0.2668	0.0512	10
		F_7	0.4554	0.0873	4
A_3	0.2367	F_8	0.2417	0.0572	6
		F_9	0.7583	0.1795	1
A_4	0.3173	F_{10}	0.1978	0.0628	5
		F_{11}	0.1567	0.0497	12
		F_{12}	0.1108	0.0352	13
		F_{13}	0.1615	0.0512	9
		F_{14}	0.0863	0.0274	14

	F_{15}	0.2869	0.0910	3

5.3. Ranking the Material Alternatives Using the MABAC Method

By applying the fuzzy MABAC procedures described in Section 4.3, the final ranking and optimal choice of each composite material were determined as follows: (1) using Equation (27), a normalized fuzzy decision matrix was constructed, which is shown in Table A3; (2) the weighted matrix and the BAA matrix were obtained through Equations (28) and (29); (3) based on Equation (30), the distance matrix D was calculated; (4) the comprehensive evaluation value of Q_i (i = 1, 2, …, 21) was obtained using Equation (31), as summarized in Table 9. The ranking results of all alternatives were obtained. Therefore, the best alternative was identified as S_{16}: S-CCFRC (50 °C –4 h).

Table 9. Rank of the options based on MABAC evaluation.

Alternative	Q_i	Rank	Alternative	Q_i	Rank
S_1	0.0637	9	S_{12}	−0.0798	19
S_2	0.0350	11	S_{13}	0.0696	8
S_3	0.0018	15	S_{14}	0.0286	12
S_4	−0.0273	18	S_{15}	0.1451	3
S_5	−0.1476	21	S_{16}	0.1668	1
S_6	0.0017	16	S_{17}	0.1477	2
S_7	−0.0033	17	S_{18}	0.0265	13
S_8	0.1117	5	S_{19}	−0.0826	20
S_9	0.0937	6	S_{20}	0.1193	4
S_{10}	0.0554	10	S_{21}	0.0769	7
S_{11}	0.0220	14			

5.4. Sensitivity Analysis

To examine the impact of changes in criterion weights on the final results, 19 sensitivity analysis cases were conducted, and the experimental setup is shown in Figure 4. The change in composite ranking was observed by the fuzzy MABAC method. For the first 15 tests, each single criterion was assigned the highest weight, while all the other criteria were assigned the same, lower weight. In test 16, each criterion that falls into the economic attribute group (F_1–F_4) was assigned to a weight of 1/4, and all other criteria were assigned a weight of 0. Test 17 put focus on environmental attribute criteria (F_5–F_7): each of these was assigned a weight of 1/3, while any criteria not related to the environment were set to 0. Test 18 dealt with social attribute criteria (F_8–F_9), with each given a weight of 0.5 and all other criteria weighted at 0. Test 19 targeted mechanical property criteria (F_{10}–F_{15}); each was allocated a weight of 1/6, and all the rest were set to 0. The findings derived from these sensitivity analyses are documented in Table A4 and illustrated through the data in Figure 7. These visual and tabular representations demonstrate how fluctuations in input parameters influence the overall reliability of the model.

Based on the research findings laid out above, several key conclusions can be made: (1) Tweaks to the weight given to each evaluation index bring about big shifts in the final ranking of candidate materials. Thus, setting up a reasonable multi-criteria weight calculation framework that fits specific engineering scenarios and needs is really important. (2) S_1: Matrix (Untreated) has the highest score when the criteria, i.e., F_1, F_2, F_3, F_4, F_5, F_6, F_8, F_{14} and F_{15}, reach a larger proportion. In addition, S_{16} has a great advantage in mechanical properties (F_{10}–F_{15}). The decrease in the proportion of mechanical properties reduces the decision result of S_{16}. It is worth noting that big changes to the indicator system itself will also set off dramatic shifts in material rankings, which shows that a well-designed, scientific evaluation framework can act as a useful decision-making tool.

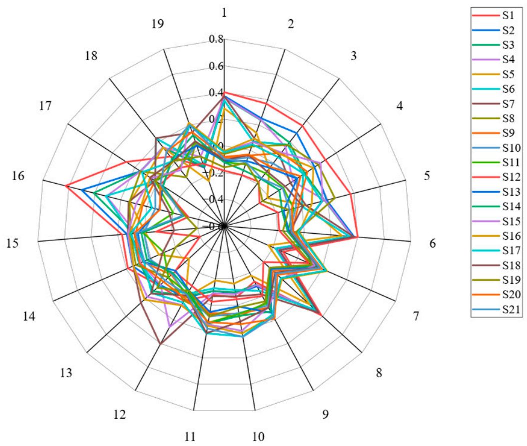

Figure 7. The results of sensitivity analysis.

5.5. Validation and Practical Implications

To check whether the proposed approach works better, a comparative analysis was conducted using three other fuzzy MCDM methods: fuzzy TOPSIS, fuzzy VIKOR, and fuzzy TODIM. It should be emphasized that the same indicator weight assignments were applied across all four methods, thereby enabling the influence of different decision-making frameworks on ranking outcomes to be clearly isolated and highlighted. Table 10 illustrates the material rankings obtained by all four methods. By presenting these results side-by-side, the data highlight the consistency and variation found among the four methods.

Table 10. Rank results of the four methods.

Methods	Ranking Result
Fuzzy TOPSIS (M_1)	$S_{16} > S_{17} > S_{20} > S_{15} > S_9 > S_{13} > S_8 > S_{10} > S_{21} > S_{14} > S_{11} > S_{18} > S_{12} > S_{19} > S_6 > S_2 > S_1 > S_3 > S_7 > S_4 > S_5$
Fuzzy VIKOR (M_2)	$S_{16} > S_{17} > S_{15} > S_{20} > S_8 > S_9 > S_{13} > S_{21} > S_{10} > S_1 > S_{18} > S_{14} > S_{11} > S_2 > S_6 > S_7 > S_3 > S_4 > S_{12} > S_{19} > S_5$
Fuzzy TODIM (M_3)	$S_{16} > S_{15} > S_{17} > S_1 > S_7 > S_2 > S_8 > S_{20} > S_4 > S_3 > S_6 > S_9 > S_{10} > S_{21} > S_{18} > S_{13} > S_{11} > S_{14} > S_{12} > S_{19} > S_5$
Our proposed method (M_4)	$S_{16} > S_{17} > S_{15} > S_{20} > S_8 > S_9 > S_{21} > S_{13} > S_1 > S_{10} > S_2 > S_{14} > S_{18} > S_{11} > S_3 > S_6 > S_7 > S_4 > S_{12} > S_{19} > S_5$

As Table 10 shows, all four methods identity S_{16} as the best material candidate and S_5: Matrix (200 °C–4 h) as the worst option. This consistency indicates that the TFN–FUCOM–ITARA–MABAC method is effective and reliable. A closer look at methods M_1, M_2 and M_4 finds that all three are based on the core idea of measuring the distance between alternative candidates, which is why their final rankings are similar. The main difference is their sensitivity to measurement scale changes in fuzzy theory: M_1's ranking results change with shifts to the fuzzy measurement scale, while M_2 and M_4 can produce stable, consistent results that are not affected by such scale adjustments. As a result, the ranking results of M_2 and M_4 are more similar, whereas M_2 usually provides compromise solutions, so that the optimal choice of M_4 is more reliable. The reason for the large gap between the ranking results of M_3 and M_4 is that M_3 only considers the degree of relative advantage and ignores the distance metric between the alternatives at the global scale, so the mechanical advantages of some CCFRCs alternatives are not sufficiently taken into account, leading to a higher ranking of some matrices that are dominant in economic level.

To quantitatively assess the consistency among different methods, Spearman's rank correlation analysis was further conducted. Taking the proposed method M_4 as the benchmark, the Spearman's rank correlation coefficients are 0.984 between M_4 and fuzzy M_2, indicating extremely high consistency; 0.862 between M_4 and M_1, indicating strong consistency; and 0.640 between M_4 and M_3, indicating moderate consistency. These findings further verify the robustness and reliability of the proposed method.

The data presented in Table A_4 indicate that each attribute contributes differently to the final outcome. Specifically, attribute A_4 (with a weight of 0.3173) and attribute A_1 (with a weight of 0.2542) exert the most substantial impact. In addition, a study on the floor of high-speed trains showed that production efficiency (F_9) (0.1795), power consumption (F_4) (0.1278), and relative change in thickness (F_{15}) (0.0910) exerted a significant effect on material selection.

The experimental observations further support the ranking obtained by the pro-posed M_4 method. Under suitable heat treatment conditions, CCFRCs exhibit improved dimensional stability, contributing to enhanced mechanical performance. Meanwhile, S-CCFRCs exhibit superior mechanical properties compared with C-CCFRCs. The experimentally observed superior mechanical performance of S-CCFRCs is consistent with the MCDM evaluation. Since mechanical property (A_4) has the highest weight in the evaluation, and all criteria are comprehensively considered, the proposed MCDM framework identifies S_{16}, representing the S-CCFRC processed at 50 °C for 4 h, as the optimal alternative.

The selected material (S_{16}) provides balanced performance in lightweight characteristics, energy consumption, production efficiency, and mechanical properties, making it suitable for train floor structures requiring reduced weight and reliable structural performance. Therefore, the proposed decision framework can provide practical guidance for material selection in railway engineering. In addition, it can be extended to other fiber-reinforced composite applications, such as automotive and aerospace structures, where similar multi-criteria trade-offs exist among mechanical properties, manufacturability, and energy efficiency, and it requires domain-specific evaluation indicator systems.

The practical implications derived from this research are summarized in three main aspects: (1) It systematically examines how varying temperatures and durations of heat treatment influence the dimensional stability and flexural mechanical properties of 3D-printed CCF composites, with a focus on both concentrated and dispersed CCF layer configurations. (2) It constructs a complete multi-criteria model that systematically considers economic, environmental, social and mechanical properties as well as heat treatment context. (3) It proposes a hybrid decision method on composite material selection in a fuzzy environment. The presented FUCOM–ITARA weighting method effectively solves decision problems where a large number of indicators exist, avoiding the influence of insufficient expert knowledge and personal preferences. Furthermore, TFN theory is applied to appropriately account for measurement uncertainties and reduces the influence of experimental fluctuations on the final selection results. The findings of this study can more effectively assist production personnel in addressing material selection challenges for composite materials.

6. Conclusions

3D printing is a transformative manufacturing technology with high flexibility, customization capability, and broad applications. However, selecting suitable composite materials remains challenging due to their complexity and the need to balance multiple properties such as tensile strength, structural rigidity, heat resistance, and production expenses. Some literature studies point out that deeper investigation into material selection for 3D-printed CCF composites under different heat treatment conditions is necessary.

This study investigated the mechanical performance of continuous-carbon-fiber-reinforced polyamide composites under six heat treatment conditions. A hierarchical evaluation index system incorporating mechanical, economic, environmental, and social criteria was developed, and a hybrid MCDM framework integrating fuzzy FUCOM–ITARA and fuzzy MABAC methods was proposed for material selection.

https://doi.org/10.3390/sym18071197

Taking the floor of a high-speed train as a case study, the proposed decision model identified S_{16} as the optimal material alternative with the highest comprehensive evaluation value of 0.1668. Among all attributes, mechanical property (A_4) exhibited the highest weight value of 0.3173, indicating that mechanical behavior plays the dominant role in the material selection process. In addition, relative change in thickness (F_{15}), power consumption (F_4), and production efficiency (F_9) also showed high importance in determining the optimal composite material, with final weights of 0.0910, 0.1278, and 0.1795, respectively.

The heat treatment experimental results provide experimental evidence supporting the MCDM evaluation results. Under suitable heat treatment conditions, CCFRCs exhibit improved dimensional stability, contributing to enhanced mechanical performance. Meanwhile, S-CCFRCs exhibit superior mechanical properties compared with C-CCFRCs. This improvement can be attributed to two factors: first, the CCF layers on the top and bottom surfaces bear higher loads; second, the scattered matrix layers undergo plastic deformation prior to the propagation of longitudinal cracks. As a result, S-CCFRC exhibits a lower crack extension rate than C-CCFRC in the bending test. S_{16} represents the S-CCFRC processed under 50 °C for 4 h heat treatment. The experimentally observed superiority of S-CCFRCs provides physical support for the MCDM results, while the proposed framework further identifies S_{16} as the optimal alternative through a comprehensive evaluation of multiple criteria.

Sensitivity analysis under 19 weighting scenarios confirms the stability of the proposed method. In addition, Spearman's rank correlation coefficients of 0.984, 0.862, and 0.640 between M_4 and M_2, M_1, and M_3, respectively, further validated the consistency and reliability of the proposed method. This research provided a high-efficiency evaluative framework for addressing the difficulties of composite material selection, while also providing a theoretical basis for production personnel.

Future research emerging from this work will focus on two primary avenues: (1) exploring different 3D-printed composites and additional material process parameters; (2) using experimental test results as much as possible instead of expert evaluation scores to reduce the influence of subjectivity in specialist assessments on the final results.

Author Contributions: Writing—original draft, H.Z. and S.Z.; conceptualization, H.Z., S.Z., W.Z. and L.W.; methodology, H.Z. and L.W.; validation, W.Z., Y.P. and K.W.; formal analysis, Y.P. and K.W.; investigation, L.W. All authors have read and agreed to the published version of the manuscript.

Funding: This research was funded by the Young Talent of Lifting Engineering for Science and Technology in Shandong, China (Grant No. SDAST2024QTA054), and the Key R&D Program of Shandong Province (Grant No. 2024CXGC010301).

Data Availability Statement: The original contributions presented in this study are included in the article.

Conflicts of Interest: The authors declare no conflicts of interest.

Appendix A

Table A1. Linguistic assessment of the expert's opinion. (This table presents the evaluation scores of material alternatives under the remaining criteria (F_2, F_3, F_5, F_6 and F_7), where expert assessments are conducted based on the linguistic assessment scales.)

	Economic Perspective		Environmental Perspective		
	Maintenance Cost	**Disposal Cost**	**Environmental Protection**	**Raw Material Extraction**	**Potential for Recycling and Reuse**
			Onyx		
Untreated (S_1)	VL	VL	SL	M	L
50 °C–4 h (S_2)	L	L	SL	M	L
100 °C–4 h (S_3)	L	SL	SL	M	L
150 °C–4 h (S_4)	L	M	SL	M	L
200 °C–4 h (S_5)	L	SH	SL	M	L
50 °C–8 h (S_6)	M	SL	L	M	L
100 °C–8 h (S_7)	M	SH	L	M	L
			C-CCFRCs		
Untreated (S_8)	SH	SL	M	H	H
50 °C–4 h (S_9)	H	M	L	H	H
100 °C–4 h (S_{10})	H	SH	L	H	H
150 °C–4 h (S_{11})	H	H	L	H	H
200 °C–4 h (S_{12})	VH	VH	L	H	H
50 °C–8 h (S_{13})	VH	SH	VL	H	H
100 °C–8 h (S_{14})	VH	VH	VL	H	H
			S-CCFRCs		
Untreated (S_{15})	M	SL	M	H	H
50 °C–4 h (S_{16})	SH	M	L	H	H
100 °C–4 h (S_{17})	SH	SH	L	H	H
150 °C–4 h (S_{18})	SH	H	L	H	H
200 °C–4 h (S_{19})	SH	VH	L	H	H
50 °C–8 h (S_{20})	H	SH	VL	H	H
100 °C–8 h (S_{21})	H	VH	VL	H	H

https://doi.org/10.3390/sym18071197

Table A2. The fuzzy decision matrix of material alternatives. (This table presents the aggregated fuzzy decision matrix obtained by integrating the evaluations of three experts using triangular fuzzy numbers.)

	F_1	F_2	F_3	F_4	F_5	F_6	F_7	F_8	F_9	F_{10}	F_{11}	F_{12}	F_{13}	F_{14}	F_{15}
S_1	(0.77, 0.77, 0.77)	(0, 0, 5)	(0, 0, 1)	(0.000, 0.000, 0.000)	(1, 4.7177, 9)	(3, 5, 7)	(0, 1.4422, 5)	(3.82, 3.82, 3.82)	(34, 34, 34)	(550.08, 593.18, 636.28)	(23.26, 24.89, 26.52)	(0.00, 0.00, 0.00)	(4.97, 5.61, 6.25)	(0.00, 0.00, 0.00)	(0.00, 0.00, 0.00)
S_2	(0.77, 0.77, 0.77)	(0, 2.4662, 7)	(0, 1, 3)	(0.343, 0.343, 0.343)	(1, 3, 5)	(3, 5, 7)	(0, 1.4422, 5)	(3.82, 3.82, 3.82)	(38, 38, 38)	(490.10, 528.38, 566.66)	(22.69, 24.71, 26.73)	(0.00, 0.00, 0.00)	(5.49, 6.07, 6.65)	(0.00, 0.17, 0.34)	(0.17, 0.34, 0.51)
S_3	(0.77, 0.77, 0.77)	(0, 2.4662, 7)	(1, 3, 5)	(0.706, 0.706, 0.706)	(1, 3, 5)	(3, 5, 7)	(0, 1.4422, 5)	(3.82, 3.82, 3.82)	(38, 38, 38)	(644.94, 726.42, 807.90)	(32.09, 34.69, 37.29)	(0.00, 0.00, 0.00)	(7.46, 7.95, 8.44)	(0.66, 0.82, 0.98)	(1.56, 2.16, 2.76)
S_4	(0.77, 0.77, 0.77)	(0, 2.4662, 7)	(1, 4.2172, 7)	(1.252, 1.252, 1.252)	(1, 3, 5)	(3, 5, 7)	(0, 1.4422, 5)	(3.82, 3.82, 3.82)	(38, 38, 38)	(989.15, 1109.86, 1230.57)	(41.02, 44.05, 47.08)	(0.16, 0.17, 0.18)	(5.97, 6.24, 6.51)	(0.84, 0.94, 1.04)	(2.40, 2.81, 3.22)
S_5	(0.77, 0.77, 0.77)	(0, 2.7589, 9)	(5, 7, 9)	(1.983, 1.983, 1.983)	(0, 2.0801, 5)	(3, 5, 7)	(0, 1.4422, 5)	(3.82, 3.82, 3.82)	(38, 38, 38)	(1143.88, 1190.19, 1236.50)	(32.10, 32.90, 33.70)	(0.06, 0.06, 0.06)	(1.43, 1.49, 1.55)	(1.81, 1.98, 2.15)	(1.72, 2.31, 2.90)
S_6	(0.77, 0.77, 0.77)	(3, 6.0822, 10)	(1, 3, 5)	(0.686, 0.686, 0.686)	(0, 1, 3)	(3, 5, 7)	(0, 1.4422, 5)	(3.82, 3.82, 3.82)	(42, 42, 42)	(748.18, 785.30, 822.42)	(31.04, 34.20, 37.36)	(0.00, 0.00, 0.00)	(6.69, 7.24, 7.79)	(0.18, 0.43, 0.68)	(0.04, 0.39, 0.74)
S_7	(0.77, 0.77, 0.77)	(3, 6.2996, 10)	(3, 6.2573, 9)	(1.412, 1.412, 1.412)	(0, 1, 3)	(3, 5, 7)	(0, 1.4422, 5)	(3.82, 3.82, 3.82)	(42, 42, 42)	(1281.57, 1458.47, 1635.37)	(49.70, 53.44, 57.18)	(0.20, 0.26, 0.32)	(8.55, 10.58, 12.61)	(0.13, 0.22, 0.31)	(0.47, 0.57, 0.67)
S_8	(4.71, 4.71, 4.71)	(5, 7, 9)	(1, 3, 5)	(0, 0, 0)	(1, 4.2172, 7)	(7, 9, 10)	(3, 7.3986, 10)	(3.60, 3.60, 3.60)	(48, 48, 48)	(8949.53, 8985.22, 9020.91)	(168.12, 168.96, 169.80)	(0.03, 0.04, 0.05)	(4.39, 5.01, 5.63)	(0.00, 0.00, 0.00)	(0.00, 0.00, 0.00)
S_9	(4.71, 4.71, 4.71)	(5, 8.2768, 10)	(1, 4.2172, 7)	(0.343, 0.343, 0.343)	(0, 1, 3)	(7, 9, 10)	(7, 9, 10)	(3.60, 3.60, 3.60)	(52, 52, 52)	(8887.86, 9246.96, 9606.06)	(175.75, 182.00, 188.25)	(0.03, 0.03, 0.03)	(4.41, 4.95, 5.49)	(0.19, 0.44, 0.69)	(0.20, 0.39, 0.58)
S_{10}	(4.71, 4.71, 4.71)	(5, 8.2768, 10)	(3, 6.2573, 9)	(0.706, 0.706, 0.706)	(0, 1, 3)	(7, 9, 10)	(7, 9, 10)	(3.60, 3.60, 3.60)	(52, 52, 52)	(9531.39, 9629.19, 9726.99)	(203.42, 211.32, 219.22)	(0.04, 0.04, 0.04)	(4.86, 5.15, 5.44)	(0.82, 0.98, 1.14)	(1.75, 2.32, 2.89)

S_{11}	(4.71, 4.71, 4.71)	(7, 9, 10)	(5, 8.2768, 10)	(1.252, 1.252, 1.252)	(0, 1, 3)	(7, 9, 10)	(7, 9, 10)	(3.60, 3.60, 3.60)	(52, 52, 52)	(10,373.61, 10,531.75, 10,689.89)	(233.18, 254.49, 275.80)	(0.04, 0.04, 0.04)	(5.98, 6.38, 6.78)	(2.26, 2.51, 2.76)	(1.19, 1.35, 1.51)
S_{12}	(4.71, 4.71, 4.71)	(7, 9.6549, 10)	(5, 8.8790, 10)	(1.983, 1.983, 1.983)	(0, 0, 3)	(7, 9, 10)	(7, 9, 10)	(3.60, 3.60, 3.60)	(52, 52, 52)	(8534.33, 8704.03, 8873.73)	(185.06, 190.27, 195.48)	(0.04, 0.04, 0.04)	(6.04, 6.37, 6.70)	(5.32, 5.89, 6.46)	(2.63, 2.74, 2.85)
S_{13}	(4.71, 4.71, 4.71)	(5, 8.8790, 10)	(5, 7, 9)	(0.686, 0.686, 0.686)	(0, 0, 1)	(7, 9, 10)	(7, 9, 10)	(3.60, 3.60, 3.60)	(56, 56, 56)	(7604.63, 7949.12, 8293.61)	(188.30, 193.95, 199.60)	(0.02, 0.02, 0.02)	(3.99, 4.51, 5.03)	(0.02, 0.11, 0.20)	(0.01, 0.11, 0.21)
S_{14}	(4.71, 4.71, 4.71)	(9, 10, 10)	(7, 9.6549, 10)	(1.412, 1.412, 1.412)	(0, 0, 1)	(7, 9, 10)	(7, 9, 10)	(3.60, 3.60, 3.60)	(56, 56, 56)	(10,479.62, 11,216.25, 11,952.88)	(241.58, 261.31, 281.04)	(0.03, 0.03, 0.03)	(5.13, 5.34, 5.55)	(0.06, 0.43, 0.80)	(0.66, 0.74, 0.82)
S_{15}	(4.73, 4.73, 4.73)	(3, 6.8041, 10)	(1, 5.1299, 10)	(0.000, 0.000, 0.000)	(0, 2.4662, 7)	(7, 9, 10)	(3, 7.3986, 10)	(3.62, 3.62, 3.62)	(49, 49, 49)	(11,014.12, 12,397.44, 13,780.76)	(201.28, 207.70, 214.12)	(0.05, 0.05, 0.05)	(8.61, 9.40, 10.19)	(0.00, 0.00, 0.00)	(0.00, 0.00, 0.00)
S_{16}	(4.73, 4.73, 4.73)	(3, 6.2573, 9)	(3, 5.5934, 9)	(0.343, 0.343, 0.343)	(0, 1.4422, 5)	(7, 9, 10)	(7, 9, 10)	(3.62, 3.62, 3.62)	(53, 53, 53)	(12,753.23, 12,996.23, 13,239.23)	(210.46, 212.27, 214.08)	(0.05, 0.05, 0.05)	(9.73, 9.98, 10.23)	(0.00, 0.085, 0.17)	(0.00, 0.69, 1.38)
S_{17}	(4.73, 4.73, 4.73)	(5, 7, 9)	(3, 6.2573, 9)	(0.706, 0.706, 0.706)	(0, 2.4662, 7)	(7, 9, 10)	(7, 9, 10)	(3.62, 3.62, 3.62)	(53, 53, 53)	(12,811.05, 14,304.91, 15,798.77)	(235.64, 257.44, 279.24)	(0.03, 0.04, 0.05)	(7.54, 8.52, 9.50)	(1.02, 1.21, 1.40)	(0.00, 0.475, 0.95)
S_{18}	(4.73, 4.73, 4.73)	(5, 7.6117, 10)	(5, 8.2768, 10)	(1.252, 1.252, 1.252)	(0, 1.4422, 5)	(7, 9, 10)	(7, 9, 10)	(3.62, 3.62, 3.62)	(53, 53, 53)	(11,900.06, 12,168.73, 12,437.40)	(270.81, 296.61, 322.41)	(0.04, 0.04, 0.04)	(8.54, 10.01, 11.48)	(2.12, 2.58, 3.04)	(9.56, 11.81, 14.06)
S_{19}	(4.73, 4.73, 4.73)	(5, 7.8837, 10)	(7, 9.6549, 10)	(1.983, 1.983, 1.983)	(0, 1, 3)	(7, 9, 10)	(7, 9, 10)	(3.62, 3.62, 3.62)	(53, 53, 53)	(8958.48, 10,054.34, 11,150.20)	(229.45, 248.04, 266.63)	(0.04, 0.05, 0.06)	(8.05, 9.87, 11.69)	(2.98, 3.31, 3.64)	(13.13, 16.74, 20.35)
S_{20}	(4.73, 4.73, 4.73)	(5, 8.2768, 10)	(5, 7.6117, 10)	(0.686, 0.686, 0.686)	(0, 0, 3)	(7, 9, 10)	(7, 9, 10)	(3.62, 3.62, 3.62)	(57, 57, 57)	(11,670.11, 11,985.86, 12,301.61)	(205.87, 223.19, 240.51)	(0.04, 0.04, 0.04)	(6.35, 6.54, 6.73)	(0.00, 0.16, 0.32)	(0.00, 0.47, 0.16)
S_{21}	(4.73, 4.73, 4.73)	(7, 9.3217, 10)	(9, 10, 10)	(1.412, 1.412, 1.412)	(0, 0, 3)	(7, 9, 10)	(7, 9, 10)	(3.62, 3.62, 3.62)	(57, 57, 57)	(15,054.29, 16,436.19, 17,818.09)	(244.82, 265.73, 286.64)	(0.02, 0.03, 0.04)	(4.95, 6.53, 8.11)	(0.46, 0.55, 0.64)	(0.14, 0.23, 0.32)
τ	0.050	0.010	0.005	0.010	0.010	0.001	0.002	0.001	0.002	0.010	0.010	0.090	0.000	0.100	0.150

Table A3. The normalized fuzzy decision matrix. (This table presents the normalized decision matrix obtained from the real decision matrix, where the values of all alternatives under each criterion are normalized to eliminate differences in measurement scales among criteria.)

Alternative	F_1	F_2	F_3	F_4	F_5	F_6	F_7	F_8	F_9	F_{10}	F_{11}	F_{12}	F_{13}	F_{14}	F_{15}
S_1	1	1	1	1	1	1	0	1	0	0.0041	6.6201×10^{-4}	0	0.4532	1	1
S_2	1	0.7803	0.8966	0.8270	0.6100	1	0	1	0.1739	0	0	0	0.5039	0.9711	0.9797
S_3	1	0.7803	0.7069	0.6440	0.6100	1	0	1	0.1739	0.0124	0.0367	0	0.7107	0.8608	0.8710
S_4	1	0.7803	0.5885	0.3686	0.6100	1	0	1	0.1739	0.0366	0.0711	0.6538	0.5226	0.8404	0.8321
S_5	1	0.7216	0.2931	0	0.4421	1	0	1	0.1739	0.0416	0.0301	0.2308	0	0.6638	0.8620
S_6	1	0.4013	0.7069	0.6541	0.2153	1	0	1	0.3478	0.0162	0.0349	0	0.6326	0.9270	0.9767
S_7	1	0.3852	0.3788	0.2879	0.2153	1	0	1	0.3478	0.0585	0.1057	1	1	0.9626	0.9659
S_8	0.0051	0.3148	0.7069	1	0.8564	0	0.7536	0	0.6087	0.5316	0.5305	0.1538	0.3872	1	1
S_9	0.0051	0.2017	0.5885	0.8270	0.2153	0	1	0	0.7826	0.5481	0.5785	0.1154	0.3806	0.9253	0.9767
S_{10}	0.0051	0.2017	0.3788	0.6440	0.2153	0	1	0	0.7826	0.5721	0.6863	0.1538	0.4026	0.8336	0.8614
S_{11}	0.0051	0.1111	0.1878	0.3686	0.2153	0	1	0	0.7826	0.6288	0.8451	0.1538	0.5380	0.5739	0.9194
S_{12}	0.0051	0.0626	0.1463	0	0.0718	0	1	0	0.7826	0.5139	0.6089	0.1538	0.5369	0	0.8363
S_{13}	0.0051	0.1571	0.2931	0.6541	0	0	1	0	0.9565	0.4665	0.6224	0.0769	0.3322	0.9813	0.9934
S_{14}	0.0051	0	0.0583	0.2879	0	0	1	0	0.9565	0.6719	0.8702	0.1154	0.4235	0.9270	0.9558
S_{15}	0	0.3478	0.4738	1	0.5692	0	0.7536	0.0909	0.6522	0.7461	0.6730	0.1923	0.8702	1	1
S_{16}	0	0.4069	0.4246	0.8270	0.3505	0	1	0.0909	0.8261	0.7838	0.6898	0.1923	0.9340	0.9856	0.9588
S_{17}	0	0.3148	0.3788	0.6440	0.5692	0	1	0.0909	0.8261	0.8660	0.8559	0.1538	0.7734	0.7946	0.9716
S_{18}	0	0.2510	0.1878	0.3686	0.3505	0	1	0.0909	0.8261	0.7317	1	0.1538	0.9373	0.5620	0.2945
S_{19}	0	0.2308	0.0583	0	0.2153	0	1	0.0909	0.8261	0.5988	0.8214	0.1923	0.9219	0.4380	0
S_{20}	0	0.2017	0.2337	0.6541	0.0718	0	1	0.0909	1	0.7202	0.7300	0.1538	0.5556	0.9728	0.9797
S_{21}	0	0.0873	0	0.2879	0.0718	0	1	0.0909	1	1	0.8864	0.1154	0.5545	0.9066	0.9863

Table A4. Sensitivity analysis results. (This table reports the results of 19 sensitivity analysis cases, showing the variations in ranking results of alternatives under different criterion weight settings using the proposed method.)

No.	Weight	The Integrated Index (Q_i)												
		S_1	S_2	S_3	S_4	S_5	S_6	S_7	S_8	S_9	S_{10}	S_{11}	S_{12}	S_{13}
1	$\omega_{F1} = 0.44$, $\omega_{F2–F15} = 0.04$	0.4015	0.3729	0.3594	0.3623	0.2815	0.3397	0.3715	−0.0608	−0.0890	−0.1053	−0.1216	−0.1861	−0.1132
2	$\omega_{F2} = 0.44$, $\omega_{F1,F3–F15} = 0.04$	0.3690	0.2525	0.2391	0.2420	0.1377	0.0678	0.0931	0.0306	−0.0428	−0.0591	−0.1116	−0.1955	−0.0849

https://doi.org/10.3390/sym18071197

3	$\omega_{F3} = 0.44$, $\omega_{F1–F2,F4–F15} = 0.04$	0.3511	0.2811	0.1918	0.1473	−0.0516	0.1720	0.0726	0.1695	0.0939	−0.0062	−0.0989	−0.1800	−0.0484
4	$\omega_{F4} = 0.44$, $\omega_{F1–F3,F5–F15} = 0.04$	0.3042	0.2064	0.1197	0.0124	−0.2158	0.1040	−0.0106	0.2398	0.1425	0.0530	−0.0735	−0.2854	0.0490
5	$\omega_{F5} = 0.44$, $\omega_{F1–F4,F6–F15} = 0.04$	0.3744	0.1897	0.1763	0.1792	0.0312	−0.0013	0.0305	0.2526	−0.0320	−0.0483	−0.0647	−0.1865	−0.1424
6	$\omega_{F6} = 0.44$, $\omega_{F1–F5,F7–F15} = 0.04$	0.4024	0.3737	0.3603	0.3631	0.2824	0.3405	0.3723	−0.0620	−0.0902	−0.1065	−0.1228	−0.1872	−0.1144
7	$\omega_{F7} = 0.44$, $\omega_{F1–F6,F8–F15} = 0.04$	−0.1207	−0.1494	−0.1628	−0.1599	−0.2407	−0.1826	−0.1507	0.1163	0.1867	0.1704	0.1541	0.0897	0.1625
8	$\omega_{F8} = 0.44$, $\omega_{F1–F7,F9–F15} = 0.04$	0.3875	0.3589	0.3455	0.3483	0.2676	0.3257	0.3575	−0.0769	−0.1050	−0.1213	−0.1376	−0.2021	−0.1293
9	$\omega_{F9} = 0.44$, $\omega_{F1–F8,F10–F15} = 0.04$	−0.1275	−0.0865	−0.1000	−0.0971	−0.1779	−0.0502	−0.0184	0.0516	0.0930	0.0767	0.0604	−0.0040	0.1384
10	$\omega_{F10} = 0.44$, $\omega_{F1–F9,F11–F15} = 0.04$	−0.0582	−0.0884	−0.0969	−0.0844	−0.1631	−0.1152	−0.0664	0.0885	0.0669	0.0602	0.0666	−0.0438	0.0100
11	$\omega_{F11} = 0.44$, $\omega_{F1–F10,F12–F15} = 0.04$	−0.0790	−0.1079	−0.1067	−0.0901	−0.1872	−0.1272	−0.0671	0.0685	0.0596	0.0864	0.1336	−0.0253	0.0529
12	$\omega_{F12} = 0.44$, $\omega_{F1–F11,F13–F15} = 0.04$	0.0375	0.0089	−0.0046	0.2598	0.0098	−0.0243	0.4075	0.0346	−0.0089	−0.0098	−0.0261	−0.0906	−0.0485
13	$\omega_{F13} = 0.44$, $\omega_{F1–F12,F14–F15} = 0.04$	0.0598	0.0514	0.1207	0.0483	−0.2415	0.0697	0.2485	−0.0310	−0.0618	−0.0693	−0.0315	−0.0964	−0.1054
14	$\omega_{F14} = 0.44$, $\omega_{F1–F13,F15} = 0.04$	0.1882	0.1481	0.0905	0.0852	−0.0662	0.0972	0.1433	0.1239	0.0658	0.0129	−0.1074	−0.4014	0.0640
15	$\omega_{F15} = 0.44$, $\omega_{F1–F14} = 0.04$	0.1679	0.1311	0.0742	0.0615	−0.0073	0.0967	0.1242	0.1035	0.0660	0.0036	0.0105	−0.0872	0.0485
16	$\omega_{F1–F4} = 0.25$, $\omega_{F5–F15} = 0$	0.6253	0.5013	0.4081	0.3097	0.1290	0.3159	0.1383	0.1320	0.0309	−0.0673	−0.2065	−0.3212	−0.0973
17	$\omega_{F5–F7} = 0.33$, $\omega_{F1–F4,F8–F15} = 0$	0.2781	0.1493	0.1493	0.1493	0.0939	0.0191	0.0191	0.1494	0.0191	0.0191	0.0191	−0.0283	−0.0519
18	$\omega_{F8–F9} = 0.50$, $\omega_{F1–F7,F10–F15} = 0$	0.0593	0.1462	0.1462	0.1462	0.1462	0.2332	0.2332	−0.1364	−0.0494	−0.0494	−0.0494	−0.0494	0.0375
19	$\omega_{F10–F15} = 0.17$, $\omega_{F1–F9} = 0$	−0.1368	−0.1373	−0.1311	−0.0520	−0.2438	−0.1148	0.1411	0.0579	0.0446	0.0421	0.0674	−0.1041	0.0358

No.	Weight	The Integrated Index (Q_i)								Rank
		S_{14}	S_{15}	S_{16}	S_{17}	S_{18}	S_{19}	S_{20}	S_{21}	
1	$\omega_{F1} = 0.44$, $\omega_{F2–F15} = 0.04$	−0.1239	−0.0420	−0.0380	−0.0472	−0.1066	−0.1611	−0.0822	−0.0973	1 > 2 > 7 > 4 > 3 > 6 > 5 > 16 > 15 > 17 > 8 > 20 > 9 > 21 > 10 > 18 > 13 > 11 > 14 > 19 > 12
2	$\omega_{F2} = 0.44$, $\omega_{F1,F3–F15} = 0.04$	−0.1584	0.0646	0.0923	0.0462	−0.0387	−0.1012	−0.0340	−0.0949	1 > 2 > 4 > 3 > 5 > 7 > 16 > 6 > 15 > 17 > 8 > 20 > 18 > 9 > 10 > 13 > 21 > 19 > 11 > 14 > 12
3	$\omega_{F3} = 0.44$, $\omega_{F1–F2,F4–F15} = 0.04$	−0.1531	0.0971	0.0814	0.0539	−0.0819	−0.1882	−0.0392	−0.1477	1 > 2 > 3 > 6 > 8 > 4 > 15 > 9 > 16 > 7 > 17 > 10 > 20 > 13 > 5 > 18 > 11 > 21 > 14 > 12 > 19
4	$\omega_{F4} = 0.44$, $\omega_{F1–F3,F5–F15} = 0.04$	−0.1081	0.2606	0.1955	0.1130	−0.0565	−0.2584	0.0821	−0.0795	1 > 15 > 8 > 2 > 16 > 9 > 3 > 17 > 6 > 20 > 10 > 13 > 4 > 7 > 18 > 11 > 21 > 14 > 5 > 19 > 12
5	$\omega_{F5} = 0.44$, $\omega_{F1–F4,F6–F15} = 0.04$	−0.1531	0.1585	0.0751	0.1533	0.0064	−0.1021	−0.0807	−0.0958	1 > 8 > 2 > 4 > 3 > 15 > 17 > 16 > 5 > 7 > 18 > 6 > 9 > 10 > 11 > 20 > 21 > 19 > 13 > 14 > 12
6	$\omega_{F6} = 0.44$, $\omega_{F1–F5,F7–F15} = 0.04$	−0.1251	−0.0412	−0.0372	−0.0464	−0.1058	−0.1602	−0.0814	−0.0965	1 > 2 > 7 > 4 > 3 > 6 > 5 > 16 > 15 > 17 > 8 > 20 > 9 > 21 > 18 > 10 > 13 > 11 > 14 > 19 > 12
7	$\omega_{F7} = 0.44$, $\omega_{F1–F6,F8–F15} = 0.04$	0.1518	0.1371	0.2397	0.2305	0.1711	0.1167	0.1955	0.1804	16 > 17 > 20 > 9 > 21 > 18 > 10 > 13 > 11 > 14 > 15 > 19 > 8 > 12 > 1 > 2 > 7 > 4 > 3 > 6 > 5

8	$\omega_{F8} = 0.44$, $\omega_{F1–F7,F9–F15} = 0.04$	−0.1399	−0.0197	−0.0156	−0.0249	−0.0843	−0.1387	−0.0599	−0.0750	1 > 2 > 7 > 4 > 3 > 6 > 5 > 16 > 15 > 17 > 20 > 21 > 8 > 18 > 9 > 10 > 13 > 11 > 19 > 14 > 12
9	$\omega_{F9} = 0.44$, $\omega_{F1–F8,F10–F15} = 0.04$	0.1277	0.0898	0.1634	0.1542	0.0948	0.0404	0.1888	0.1737	20 > 21 > 16 > 17 > 13 > 14 > 18 > 9 > 15 > 10 > 11 > 8 > 19 > 12 > 7 > 6 > 2 > 4 > 3 > 1 > 5
10	$\omega_{F10} = 0.44$, $\omega_{F1–F9,F11–F15} = 0.04$	0.0815	0.1951	0.2142	0.2378	0.1247	0.0171	0.1445	0.2413	21 > 17 > 16 > 15 > 20 > 18 > 8 > 14 > 9 > 11 > 10 > 19 > 13 > 12 > 1 > 7 > 4 > 2 > 3 > 6 > 5
11	$\omega_{F11} = 0.44$, $\omega_{F1–F10,F12–F15} = 0.04$	0.1413	0.1463	0.1571	0.2143	0.2125	0.0867	0.1289	0.1764	17 > 18 > 21 > 16 > 15 > 14 > 11 > 20 > 19 > 10 > 8 > 9 > 13 > 12 > 7 > 1 > 4 > 3 > 2 > 6 > 5
12	$\omega_{F12} = 0.44$, $\omega_{F1–F11,F13–F15} = 0.04$	−0.0438	0.0708	0.0749	0.0503	−0.0091	−0.0482	0.0153	−0.0152	7 > 4 > 16 > 15 > 17 > 1 > 8 > 20 > 5 > 2 > 3 > 9 > 18 > 10 > 21 > 6 > 11 > 14 > 19 > 13 > 12
13	$\omega_{F13} = 0.44$, $\omega_{F1–F12,F14–F15} = 0.04$	−0.0796	0.1830	0.2126	0.1391	0.1453	0.0847	0.0170	0.0014	7 > 16 > 15 > 18 > 17 > 3 > 19 > 6 > 1 > 2 > 4 > 20 > 21 > 8 > 11 > 9 > 10 > 14 > 12 > 13 > 5
14	$\omega_{F14} = 0.44$, $\omega_{F1–F13,F15} = 0.04$	0.0316	0.1447	0.1429	0.0573	−0.0951	−0.1991	0.0936	0.0520	1 > 2 > 15 > 7 > 16 > 8 > 6 > 20 > 3 > 4 > 9 > 13 > 17 > 21 > 14 > 10 > 5 > 18 > 11 > 19 > 12
15	$\omega_{F15} = 0.44$, $\omega_{F1–F14} = 0.04$	0.0227	0.1243	0.1119	0.1078	−0.2225	−0.3947	0.0760	0.0635	1 > 2 > 15 > 7 > 16 > 17 > 8 > 6 > 20 > 3 > 9 > 21 > 4 > 13 > 14 > 11 > 10 > 5 > 12 > 18 > 19
16	$\omega_{F1–F4} = 0.25$, $\omega_{F5–F15} = 0$	−0.2868	0.0808	0.0400	−0.0403	−0.1728	−0.3024	−0.1023	−0.2808	1 > 2 > 3 > 6 > 4 > 7 > 8 > 5 > 15 > 16 > 9 > 17 > 10 > 13 > 20 > 18 > 11 > 21 > 14 > 19 > 12
17	$\omega_{F5–F7} = 0.33$, $\omega_{F1–F4,F8–F15} = 0$	−0.0519	0.0546	0.0637	0.1359	0.0637	0.0191	−0.0283	−0.0283	1 > 8 > 2 > 3 > 4 > 17 > 5 > 16 > 18 > 15 > 6 > 7 > 9 > 10 > 11 > 19 > 12 > 20 > 21 > 13 > 14
18	$\omega_{F8–F9} = 0.50$, $\omega_{F1–F7,F10–F15} = 0$	0.0375	−0.0692	0.0178	0.0178	0.0178	0.0178	0.1047	0.1047	6 > 7 > 2 > 3 > 4 > 5 > 20 > 21 > 1 > 13 > 14 > 16 > 17 > 18 > 19 > 9 > 10 > 11 > 12 > 15 > 8
19	$\omega_{F10–F15} = 0.17$, $\omega_{F1–F9} = 0$	0.1192	0.2073	0.2179	0.1960	0.0709	−0.0493	0.1444	0.2017	16 > 15 > 21 > 17 > 20 > 7 > 14 > 18 > 11 > 8 > 9 > 10 > 13 > 19 > 4 > 12 > 6 > 3 > 1 > 2 > 5

References

1. Liu, F.; Ferraris, E.; Ivens, J. Mechanical investigation and microstructure performance of a two–matrix continuous carbon fibre composite fabricated by 3D printing. *J. Manuf. Process.* **2022**, *79*, 383–393. https://doi.org/10.1016/j.jmapro.2022.04.050.
2. Peng, X.; Kuang, X.; Roach, D.J.; Wang, Y.; Hamel, C.M.; Lu, C.; Qi, H.J. Integrating digital light processing with direct ink writing for hybrid 3D printing of functional structures and devices. *Addit. Manuf.* **2021**, *40*, 101911. https://doi.org/10.1016/j.addma.2021.101911.
3. Guo, H.; Zhao, H.; Niu, H.; Ren, Y.; Fang, H.; Fang, X.; Lv, R.; Maqbool, M.; Bai, S. Highly Thermally Conductive 3D Printed Graphene Filled Polymer Composites for Scalable Thermal Management Applications. *ACS Nano* **2021**, *15*, 6917–6928. https://doi.org//10.1021/acsnano.0c10768.
4. Khan, S.J.; Albishri, N.; Galgotia, A.; Papa, A. 3D printing technologies and innovation performance. An agile manufacturing theory perspective. *Technovation* **2026**, *149*, 103347. https://doi.org/10.1016/j.technovation.2025.103347.
5. Alarifi, I.M. Revolutionising fabrication advances and applications of 3D printing with composite materials: A review. *Virtual Phys. Prototyp.* **2024**, *19*, e2390504. https://doi.org/10.1080/17452759.2024.2390504.
6. You, X.; Zhang, Q.; Yang, J.; Dong, S. Review on 3D–printed graphene–reinforced composites for structural applications. *Compos. Part A Appl. Sci. Manuf.* **2023**, *167*, 107420. https://doi.org/10.1016/j.compositesa.2022.107420.
7. Zhang, H.; Wu, Y.; Wang, K.; Peng, Y.; Wang, D.; Yao, S.; Wang, J. Materials selection of 3D–printed continuous carbon fiber reinforced composites considering multiple criteria. *Mater. Des.* **2020**, *196*, 109140. https://doi.org/10.1016/j.matdes.2020.109140.
8. Jiang, Y.; Park, S.; Lu, Z.; Bayless, J.; Kim, H. Designing resilient remanufacturing strategies: A probabilistic framework for uncertainty–aware decision making. *J. Clean. Prod*. **2026**, *539*, 147322. https://doi.org/10.1016/j.jclepro.2025.147322.
9. Sarucan, A.; Özcan, E.; Güler, B. Bonferroni Mean-Based Aggregation Operators on q-Rung Picture Fuzzy Sets for Multi-Criteria Decision Making in Energy Storage Systems. *Symmetry* **2026**, *18*, 966. https://doi.org/10.3390/sym18060966.
10. Ye, H.; Mao, P.; He, W.; Li, J.; Dong, Y.; Wang, X. Influence of process parameters on the tensile properties of CFRTP composites 3D printed structures. *Mech. Adv. Mater. Struct.* **2026**, *33*, 2440632. https://doi.org/10.1080/15376494.2024.2440632.
11. Wang, X.; Huang, L.; Li, Y.; Wang, Y.; Lu, X.; Wei, Z.; Mo, Q.; Zhang, S.; Sheng, Y.; Huang, C.; et al. Research progress in polylactic acid processing for 3D printing. *J. Manuf. Process*. **2024**, *112*, 161–178. https://doi.org/10.1016/j.jmapro.2024.01.038.
12. Wang, K.; Tan, Q.; Wang, J.; Liu, Y.; Zhai, Z.; Yao, S.; Peng, Y. A low–cost granular–medium hot quasi–isostatic pressing method for enhancing compressive properties of 3D printed structures. *J. Manuf. Process.* **2024**, *115*, 441–451. https://doi.org/10.1016/j.jmapro.2024.02.034.
13. Dickson, A.N.; Barry, J.N.; McDonnell, K.A.; Dowling, D.P. Fabrication of continuous carbon, glass and Kevlar fibre reinforced polymer composites using additive manufacturing. *Addit. Manuf.* **2017**, *16*, 146–152. https://doi.org/10.1016/j.addma.2017.06.004.
14. Justo, J.; Távara, L.; García–Guzmán, L.; París, F. Characterization of 3D printed long fibre reinforced composites. *Compos. Struct.* **2018**, *185*, 537–548. https://doi.org/10.1016/j.compstruct.2017.11.052.
15. Chacón, J.M.; Caminero, M.A.; Núñez, P.J.; García–Plaza, E.; García–Moreno, I.; Reverte, J.M. Additive manufacturing of continuous fibre reinforced thermoplastic composites using fused deposition modelling: Effect of process parameters on mechanical properties. *Compos. Sci. Technol.* **2019**, *181*, 107688. https://doi.org/10.1016/j.compscitech.2019.107688.
16. Yuan, W.; Hu, J.; Zhou, L.; Kan, Y.; Zhang, X.; Yang, J.; Xue, Y.; Chen, X.; Dong, S. Effect of fiber argon heat treatment on microstructure and properties of SiC/SiC composites prepared by CVI+RMI. *Ceram. Int.* **2025**, *51*, 31986–31995. https://doi.org/10.1016/j.ceramint.2025.04.389.
17. Wang, X.; Jiang, M.; Zhou, Z.; Gou, J.; Hui, D. 3D printing of polymer matrix composites: A review and prospective. *Compos. Part B Eng*. **2017**, *110*, 442–458. https://doi.org/10.1016/j.compositesb.2016.11.034.
18. Alshneeqat, M.G.; Abualbandora, T.A.; Mourad, A.H.I. 3D printing of short fiber reinforced polymers: A review of the materials, 3D printers, lattice structures and pre–/post–treatment impact on the mechanical characteristics. *Prog. Addit. Manuf.* **2025**, *10*, 8367–8404. https://doi.org/10.1007/s40964-025-01126-0.
19. Basgul, C.; Yu, T.; MacDonald, D.W.; Siskey, R.; Marcolongo, M.; Kurtz, S.M. Does annealing improve the interlayer adhesion and structural integrity of FFF 3D printed PEEK lumbar spinal cages? *J. Mech. Behav. Biomed. Mater.* **2020**, *102*, 103455. https://doi.org/10.1016/j.jmbbm.2019.103455.
20. Akhoundi, B.; Nabipour, M.; Hajami, F.; Shakoori, D. An Experimental Study of Nozzle Temperature and Heat Treatment (Annealing) Effects on Mechanical Properties of High-Temperature Polylactic Acid in Fused Deposition Modeling. *Polym. Eng. Sci*. **2020**, *60*, 979–987. https://doi.org/10.1002/pen.25353.
21. Bhandari, S.; Lopez–Anido, R.A.; Gardner, D.J. Enhancing the interlayer tensile strength of 3D printed short carbon fiber rein-

forced PETG and PLA composites via annealing. *Addit. Manuf.* **2019**, *30*, 100922. https://doi.org/10.1016/j.addma.2019.100922.
22. Babu, M.N.; Anandan, V.; Babu, M.D. Performance of ionic liquid as a lubricant in turning inconel 825 via minimum quantity lubrication method. *J. Manuf. Process.* **2021**, *64*, 793–804. https://doi.org/10.1016/j.jmapro.2021.02.011.
23. Fan, J.; Yao, X.; Wu, M. Extended WPA–CRITIC–WASPAS Model Based on Picture Fuzzy Soft Sets for Green Building Materials Selection. *Int. J. Fuzzy Syst.* **2026**, *8*, 701–721. https://doi.org/10.1007/s40815-025-01982-6.
24. Madhu, P.; Dhanalakshmi, C.S.; Mathew, M. Multi–criteria decision–making in the selection of a suitable biomass material for maximum bio–oil yield during pyrolysis. *Fuel* **2020**, *277*, 118109. https://doi.org/10.1016/j.fuel.2020.118109.
25. Tian, G.; Zhang, H.; Feng, Y.; Wang, D.; Peng, Y.; Jia, H. Green decoration materials selection under interior environment characteristics: A grey–correlation based hybrid MCDM method. *Renew. Sustain. Energy Rev.* **2018**, *81*, 682–692. https://doi.org/10.1016/j.rser.2017.08.050.
26. Jha, M.K.; Gupta, S.; Chaudhary, V.; Gupta, P. Material selection for biomedical application in additive manufacturing using TOPSIS approach. *Mater. Today Proc.* **2022**, *62*, 1452–1457. https://doi.org/10.1016/j.matpr.2022.01.423.
27. Wang, K.; Xie, G.; Xiang, J.; Li, T.; Peng, Y.; Wang, J.; Zhang, H. Materials selection of 3D printed polyamide-based composites at different strain rates: A case study of automobile front bumpers. *J. Manuf. Process.* **2022**, *84*, 1449–1462. https://doi.org/10.1016/j.jmapro.2022.11.024.
28. Xie, G.; Wang, K.; Wu, X.; Wang, J.; Li, T.; Peng, Y.; Zhang, H. A hybrid multi-stage decision-making method with probabilistic interval-valued hesitant fuzzy set for 3D printed composite material selection. *Eng. Appl. Artif. Intell.* **2023**, *123*, 106483. https://doi.org/10.1016/j.engappai.2023.106483.
29. Zhang, H.; Yu, D.; Hou, L.; Wang, D.; Peng, Y. Dynamic modelling and multidisciplinary injury–based design optimization of driver workspace in high–speed train collisions. *J. Ind. Inf. Integr.* **2025**, *48*, 100939. https://doi.org/10.1016/j.jii.2025.100939.
30. Wang, D.; Deng, W.; Hu, L.; Huang, Z.; Lu, Y.; Zhang, H. Safety assessment of intelligent vehicles considering drivers' risk perception information under interval 2–tuple q–rung Orthopair Fuzzy Sets. *Appl. Soft. Comput*. **2025**, *175*, 112919. https://doi.org/10.1016/j.asoc.2025.112919.
31. Dimitrellou, S.; Strantzali, E.; Iakovidis, I. A decision–making strategy for selection of FDM–based additively manufactured thermoplastics for industrial applications based on material attributes. *Sustain. Futures* **2025**, *9*, 100640. https://doi.org/10.1016/j.sftr.2025.100640.
32. Zhang, H.; Huang, Z.; Tian, G.; Wang, W.; Li, Z. A Hybrid QFD–Based Human–Centric Decision Making Approach of Disassembly Schemes Under Interval 2–Tuple q–Rung Orthopair Fuzzy Sets. *IEEE Trans. Autom. Sci. Eng.* **2023**, *22*, 724–735. https://doi.org/10.1109/TASE.2023.3301237.
33. Huang, Z.; Zhang, H.; Wang, D.; Yu, H.; Wang, L.; Yu, D.; Peng, Y. Preference–based multi–attribute decision–making method with spherical–Z fuzzy sets for green product design. *Eng. Appl. Artif. Intell*. **2023**, *126*, 106767. https://doi.org/10.1016/j.engappai.2023.106767.
34. Lyu, H.M.; Zhou, W.H.; Shen, S.L.; Zhou, A.N. Inundation risk assessment of metro system using AHP and TFN–AHP in Shenzhen. *Sustain. Cities Soc.* **2020**, *56*, 102103. https://doi.org/10.1016/j.scs.2020.102103.
35. Algawbery, A.N.; Shukri, M.A.; Al–Matwakel, M.Q. Optimizing wind plant locations in Yemen: A geospatial model using full consistency method (FUCOM). *Energy Rep.* **2026**, *15*, 109096. https://doi.org/10.1016/j.egyr.2026.109096.
36. Lo, H.W.; Chen, Y.S.; Deveci, M.; Delen, D. Objective weighting with a modified ITARA: Aspiration-Level normalization, Intercriteria dependency, and Evidence-weighted convex synthesis. *Adv. Eng. Inform*. **2026**, *72*, 104523. https://doi.org/10.1016/j.aei.2026.104523.
37. Zhang, H.; Wang, L.; Wang, D.; Huang, Z.; Yu, D.; Peng, Y. A Parameter Reduction–Based Decision–Making Method with Interval–Valued Neutrosophic Soft Sets for the Selection of Bionic Thin–Wall Structures. *Biomimetics* **2024**, *9*, 208. https://doi.org/10.3390/biomimetics9040208.
38. Mardani, A.; Zavadskas, E.K.; Govindan, K.; Senin, A.A.; Jusoh, A. VIKOR Technique: A Systematic Review of the State of the Art Literature on Methodologies and Applications. *Sustainability* **2016**, *8*, 37. https://doi.org/10.3390/su8010037.
39. Ullah, W.; Ibrar, M.; Khan, A.; Khan, M. Multiple attribute decision making problem using GRA method with incomplete weight information based on picture hesitant fuzzy setting. *Int. J. Intell. Syst.* **2021**, *36*, 866–889. https://doi.org/10.1002/int.22324.
40. Ahmmad, J.; Al–Dayel, O.A.A.; Khan, M.A.; Mahmood, T. AI–assisted technology optimization in disability support systems using fuzzy rough MABAC decision–making. *Sci. Rep.* **2025**, *15*, 18335. https://doi.org/10.1038/s41598-025-02362-8.
41. Yang, Z.; Feng, Z.; Kong, T.; Xie, J.; Zhang, Z. Optimal water and fertilizer amount for balancing greenhouse melon production efficiency and soil ecology based on TOPSIS–GRA coupling model. *Comput. Electron. Agric.* **2025**, *229*, 109797. https://doi.org/10.1016/j.compag.2024.109797.

42. Chen, Y.; Guo, J.; Qi, L.; Zhu, Y. Performance evaluation of old industrial city transformation based on the GRA–VIKOR–coupling coordination degree method. *Front. Built Environ.* **2025**, *11*, 1589016. https://doi.org/10.3389/fbuil.2025.1589016.
43. Zhang, H.; Wei, G.; Chen, X. SF–GRA method based on cumulative prospect theory for multiple attribute group decision making and its application to emergency supplies supplier selection. *Eng. Appl. Artif. Intell*. **2022**, *110*, 104679. https://doi.org/10.1016/j.engappai.2022.104679.
44. Liu, G. Uncertainty theory. *AI Soc*. **2026**, *41*, 1833–1844. https://doi.org/10.1007/s00146-025-02532-2.
45. Shen, J.; Bao, X.; Chen, X.; Wu, X.; Qiu, T.; Cui, H. Seismic resilience assessment method for tunnels based on cloud model considering multiple damage evaluation indices. *Tunn. Undergr. Space Technol.* **2025**, *157*, 106360. https://doi.org/10.1016/j.tust.2024.106360.
46. Bhong, M.; Khan, T.K.H.; Devade, K.; Krishna, B.V.; Sura, S.; Eftikhaar, H.K.; Thethi, H.P.; Gupta, N. Review of composite materials and applications. *Mater. Today Proc*. **2023**, *in press*. https://doi.org/10.1016/j.matpr.2023.10.026.
47. Zadeh, L.A. Fuzzy sets. *Inf. Control* **1965**, *8*, 338–353. https://doi.org/10.1016/S0019-9958(65)90241-X.
48. Zadeh, L.A. Outline of a New Approach to the Analysis of Complex Systems and Decision Processes. *IEEE Trans. Syst. Man Cybern.* **1973**, *SMC-3*, 28–44. https://doi.org/10.1109/TSMC.1973.5408575.
49. Govindan, K.; Khodaverdi, R.; Jafarian, A. A fuzzy multi criteria approach for measuring sustainability performance of a supplier based on triple bottom line approach. *J. Clean. Prod.* **2013**, *47*, 345–354. https://doi.org/10.1016/j.jclepro.2012.04.014.
50. Dong, J.; Wan, S.; Chen, S.M. Fuzzy best–worst method based on triangular fuzzy numbers for multi–criteria decision–making. *Inf. Sci.* **2021**, *547*, 1080–1104. https://doi.org/10.1016/j.ins.2020.09.014.
51. Wang, Z.J. Eigenproblem driven triangular fuzzy analytic hierarchy process. *Inf. Sci.* **2021**, *578*, 795–816. https://doi.org/10.1016/j.ins.2021.08.051.
52. Pamučar, D.; Stević, Ž.; Sremac, S. A new model for determining weight coefficients of criteria in mcdm models: Full consistency method (FUCOM). *Symmetry* **2018**, *10*, 393. https://doi.org/10.3390/sym10090393.
53. Hatefi, M.A. Indifference threshold–based attribute ratio analysis: A method for assigning the weights to the attributes in multiple attribute decision making. *Appl. Soft. Comput*. **2019**, *74*, 643–651. https://doi.org/10.1016/j.asoc.2018.10.050.
54. Li, P.; Xu, Z.; Wei, C.; Bai, Q.; Liu, J. A novel PROMETHEE method based on GRA–DEMATEL for PLTSs and its application in selecting renewable energies. *Inf. Sci*. **2022**, *589*, 142–161. https://doi.org/10.1016/j.ins.2021.12.090.